Charge Recombination via Long-Distance Electron Transfer through Frozen and Molten *n*-Alkyl Chains in Pulse-Irradiated Mesomorphic Phthalocyanines

Pieter G. Schouten and John M. Warman*

Radiation Chemistry Department, IRI, Delft University of Technology, Mekelweg 15, 2629 JB Delft, The Netherlands

Gerwin H. Gelinck

Department of Organic Chemistry, Nijmegen University, Toernooiveld, 6525 ED Nijmegen, The Netherlands

Marc J. Copyn

Department of Physical Organic Chemistry, Utrecht University, Padualaan 8, 3584 CH Utrecht, The Netherlands

Received: April 7, 1995[⊗]

Charge recombination following pulsed ionization of columnarly stacked, peripherally octa-*n*-alkoxy substituted phthalocyanines ("PcOC*n*" with *n* the alkyl chain length) has been studied within the time frame 10^{-9} to 10^{-2} s, from −100 to +200 °C, and for $n = 5-18$, corresponding to intercolumnar distances from 20 to 40 Å, as determined by SAXS. The first half-life of recombination obeys an exponential dependence on the edge-to-edge distance, R, between the nearest neighbor macrocyclic cores, $t_{1/2} = \tau_R \exp(\beta_R R)$, indicating intercolumnar electron tunneling to be the rate-determining step. In the solid, constant values of $\tau_R = 1.5 \times 10^{-13}$ s and $\beta_R = 1.1$ Å^{-1} are reached at low temperatures for $n = 5-18$. $t_{1/2}$ *increases* at elevated temperatures, most markedly for the shortest chains. This is attributed to "premelting" beginning at the outermost carbon atoms and resulting in conformational disorder in the interfacial region between columns. In the mesophase, for which the alkyl chains are completely molten, $\tau_R \approx 6 \times 10^{-13} \exp[0.21(\text{eV})/k_B T]$ s and $\beta_R = 0.64$ Å^{-1} for $n = 5-12$. In the mesophase of the PcOC18 compound recombination occurs preferentially by intercolumnar molecular ion diffusion rather than by electron tunneling. For all compounds the decay kinetics are disperse and can in many cases be described quite well by the Kohlrausch expression $\sigma(t) = \sigma(0) \exp(-t/\Gamma)^{\alpha}$.

Introduction

It has become universally accepted that rapid electron transfer can occur between molecular entities separated by distances much larger than their van der Waals radii.[1−14] Attention is focused at present on the precise role played by the molecular structure or medium separating the redox-active sites. This has become an area of intense theoretical and experimental investigation. Of particular relevance to the advancement of knowledge in this area is the availability of well-characterized molecular systems which can be studied in the laboratory under controlled conditions. The separation distance and, if possible, the relative orientation of the electron transfer sites in such model systems should be well-defined and remain fixed during reaction. An increasing number of such systems are becoming available in the form of either well-characterized biological structures or molecular assemblies created by the organic chemist or by self-assembling molecules themselves.

A frequent starting point for theoretical considerations has been the oligo-methylene chain as a medium via which through-bond coupling or superexchange interactions can increase the electronic coupling between distant sites and, hence, facilitate electron and hole transfer.[15−26] The simplest of σ-bonded coupling elements is, however, rather difficult to study experimentally due to its flexibility and, hence, lack of conformational integrity as a bridging unit in model donor−spacer−acceptor compounds. This problem has been alleviated to a certain extent by constructing bridges of more or less rigid aliphatic ring systems, and this type of molecule has proven invaluable in recent years for separating the effects of distance and thermodynamics on electron transfer.[2,11,27−37] Determining the "conductive" properties of the simple methylene chain remains, however, an intriguing challenge for the experimentalist. Scanning-tunneling-microscopy experiments, recently described by Rabe et al.,[38] may eventually present the best approach to this problem.

The solution to the flexibility problem has been sought up until now in the use of supramolecular assemblies of molecules with long alkyl chains, as in the pioneering work of Kuhn and Möbius.[39−42] Using Langmuir−Blodgett (LB) films of amphiphyllic molecules with alkyl chains from C_{14} to C_{22}, they demonstrated the exponential distance dependence of conduction and photoinduced charge separation through *n*-alkyl layers up to almost 30 Å thick. Applying the phenomenological relationships between electron transfer rate and either the number of methylene groups, N, or the edge-to-edge width, R_E, of the hydrocarbon barrier,

$$k_{ET} = k_N \exp(-\beta_N N) \quad (1)$$

$$= k_R \exp(-\beta_R R) \quad (2)$$

the distance dependence found corresponded to $\beta_N = 0.32$ and $\beta_R \approx 0.4$ Å^{-1}.[40] The latter value is based on the assumption of nontilted and non-intermeshed, all-trans alkyl chains in the LB layers and is, therefore, almost certainly a lower limit. Unfortunately, the accurate determination of the actual width of the alkane barrier region in this type of system is extremely difficult.

[⊗] Abstract published in *Advance ACS Abstracts,* July 1, 1995.

0022-3654/95/2099-11780$09.00/0

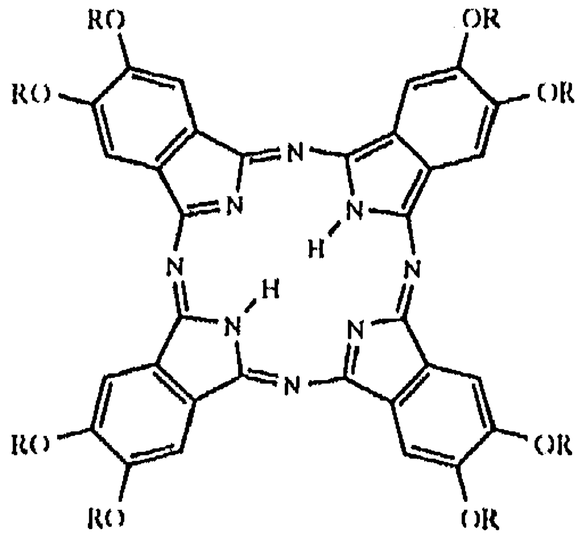

PeOCn : OR = OC_nH_{2n+1} with n = 5-12, 18

Figure 1. Primary molecular structure of the peripherally octa-*n*-alkoxy-substituted phthalocyanine derivatives studied in the present work and denoted PeOC*n*, with *n* the number of carbon atoms in the alkyl chain.

This applies also to a more recent study of electron transfer kinetics through organized thiol monolayers[43] in which β_N = 1.06 was determined and $\beta_R \approx 0.95$ Å^{-1} was estimated on the basis of the assumption of all-trans, non-interlocked alkyl chains with a tilt angle of 30°.

The above values are to be compared with β_R in the range 0.8−1.2 Å^{-1} determined for intramolecular electron transfer in "simple" molecular assemblies with cyclic alkane spacers of accurately known length.[2,3,5,11,27-35] From a consideration of a large number of electron transfer processes in protein matrixes, a general value of 1.4 Å^{-1} has been derived.[44] Considerable discussion exists, however, as to whether such generalizations can, in fact, be made.[45-47] A more detailed analysis taking into account specific pathways with consideration being given to individual contributions from through-bond and through-space barriers has been proposed.[48]

In the present work we have used the pulse-radiolysis time-resolved microwave conductivity (PR-TRMC) technique to study the kinetics of charge recombination via long-distance electron transfer in columnarly stacked, peripherally octaalkoxy substituted phthalocyanines. These supramolecular discotic materials have well-defined X-ray diffraction patterns which allow accurate estimates to be made of intra- and intercolumnar distances. The occurrence of a solid to liquid-crystal transition at which the alkyl chains melt while the columnar phthalocyanine order is retained allows one to study long-distance electron transfer through a completely disordered, liquid-like alkane medium while still retaining a well-defined edge-to-edge geometry. Additional relevance is provided by the fact that the edge-to-edge distances involved of 10−25 Å cover a range that is characteristic of many biological electron transfer systems which also often involve large macrocyclic redox centers similar to phthalocyanine.

A short, preliminary account of the recombination kinetics has been published,[49] as have articles concerned with the one-dimensional mobility of charge carriers within the macrocycle stacks.[50-52]

Materials

Figure 1 shows the primary molecular structure of the PeOC*n* compounds studied in the present work. The synthesis and characterization of these materials have been described previously.[53-59] The *n*-alkoxy-substituted derivatives all precipitate from solution as a crystalline powder at room temperature and undergo a transition from the solid to a liquid crystalline mesophase when heated. The phase transition temperatures, as obtained by differential scanning calorimetry, are given in Table 1 together with the associated enthalpy change. For comparison the melting points and enthalpies of fusion of the corresponding C_nH_{2n+2} alkane are given. The PeOC18 compound was found to have a mesophase to isotropic liquid transition at a relatively low temperature of 247 °C compared with >300 °C for the other *n*-alkoxy compounds. It also displayed flow characteristics which indicated a much lower viscosity in the mesophase.

The molecular packing of many of these disklike molecules in the solid (K) and mesophase (D) has been characterized by van der Pol et al.[54-56] using small angle X-ray diffraction (SAXS). Because of the critical importance of the X-ray information to the present study, this is discussed in detail below and divided into sections on the liquid crystalline and solid phases. Raw X-ray diffraction data are given in refs 56 and 57.

Mesophase. In the mesophase the indexation of the SAXS reflections is straightforward since the reciprocal spacings, $1/d_{hkl}$, are in the ratio $1:\sqrt{3}:\sqrt{4}:\sqrt{7}:\sqrt{9}$. This pattern is characteristic of a two-dimensional hexagonal lattice. A sharp reflection corresponding to a distance of 3.4 Å which is independent of alkyl chain length and becomes broader when the temperature is raised[54] corresponds to the intracolumnar stacking period of the Pc macrocycles. The presence of this reflection, which corresponds to the cofacial distance for aromatic π systems, demonstrates that the molecules are horizontally stacked with respect to the columnar axis. A diffuse reflection with an average spacing of 4.6 Å is attributed to the disordered aliphatic chains. Top and side views of the columnar packing in the mesophase are shown at the left in Figure 2. Table 2 lists the nearest neighbor intercolumnar center-to-center distances, *D*, calculated from the hexagonal lattice parameters.

The molecular volume for hexagonal columnar packing is given by[55,64]

$$V_m = (\sqrt{3}/2)D^2c \qquad (3)$$

with *c* the intracolumnar spacing. From this, the density of the material can be determined according to

$$\varrho = M_w/V_mN_A \qquad (4)$$

In (4) M_w is the molecular weight, and N_A Avogadro's number. The densities obtained for the present compounds are listed as ϱ_D in Table 1. In Figure 3, V_m is plotted against the number of methylene groups in the alkoxy chain, and, as might be expected,[55,64] a good linear dependence is found. From the slope, the molar volume increment per methylene group is determined to be 29 Å^3. This is very close to the values of 29.8 and 29.3 Å^3 found for similar plots for liquid *n*-alkanes and *n*-alcohols.[65] The volume increment corresponds to a density within the hydrocarbon region in the mesophase, ϱ-$(Cn)_D$ in Table 3, of 0.82 g/cm^3, showing that the region is as densely packed as a normal liquid hydrocarbon medium, for which the average density is also *ca.* 0.8 g/cm^3.[65]

The intercept of V_m at $n = 0$ is 821 Å^3. This should be a measure of the molecular volume of an octahydroxyphthalocyanine derivative. The corresponding molecular diameter is D = 17.5 Å. As would be expected, these values of V_m and D are larger than those of 587 Å^3 and 14.8 Å found for unsubstituted phthalocyanine from X-ray data.[66]

In the present work we are concerned with electron tunneling between columnar Pc stacks. An important parameter is, therefore, the nearest neighbor edge-to-edge distance between Pc macrocycles, indicated by R_D for the mesophase in Figure 2. We have derived the R_D values listed in Table 3 from the measured D values by subtracting the diameter of 14.8 Å for

TABLE 1: Characteristics of the Solid to Mesophase Transition and Comparison with Properties of *n*-Alkanes[a]

compound	T (K→D) (°C)	mp (HCn)[b] (°C)	ΔH (K→D) (kJ/mol)	$8 \times \Delta H_f$ (HCn)[b] (kJ/mol)	ϱ_K[c] (g/cm^3)	ϱ_D[d] (g/cm^3)	ref source for DSC data
PcOC5	121	−130	36	67		1.00	this work
PcOC6	119	−95	72	105	1.10	0.97	55
	102		50				58
PcOC7	104	−91	73	114		0.98	55
PcOC8	94	−57	98	165		0.95	55
	94		75				58
	96		90				59
PcOC9	101	−53	94	124	1.06	0.95	55
	107		112				this work
PcOC10	94	−30	102	230		0.94	55
PcOC11	83	−26	108	178		0.92	55
PcOC12	83	−10	109	293	1.03	0.91	55
	91		130				58,60
	91		110				59
PcOC18	98	28	239	491	1.01	0.88	this work

[a] Transition temperatures and enthalpies were determined by DSC. Symbols used: RT = room temperature; K = crystalline phase; D = discotic mesophase. [b] Reference 65. [c] At room temperature by flotation densimetry. [d] At 200 °C from SAXS with c = 3.40 Å.

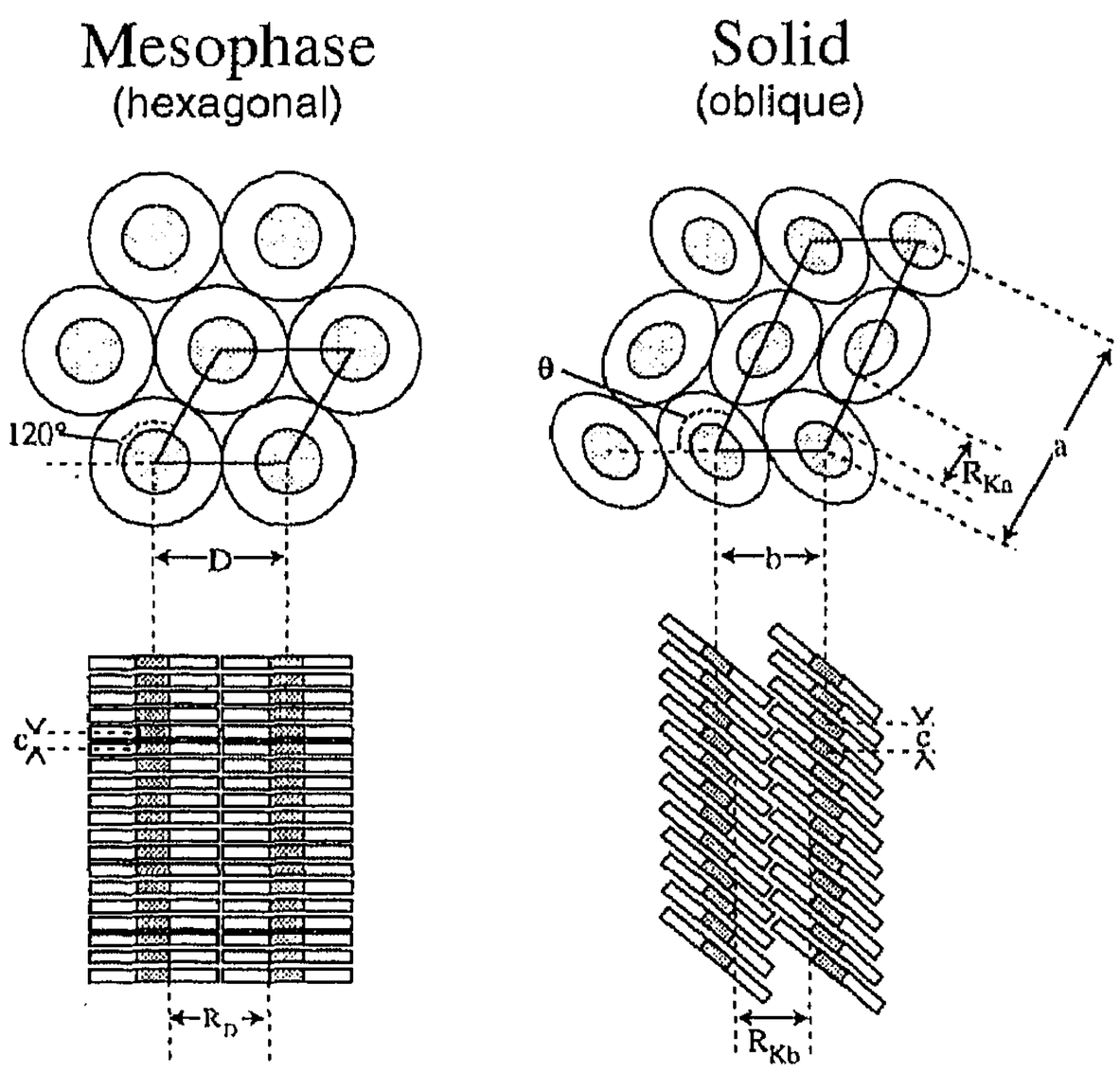

Figure 2. Secondary (columnar) and tertiary (two-dimensional lattice) structures of the PcOCn compounds showing the lattice parameters used to index the small angle X-ray (SAXS) diffraction patterns. The edge-to-edge, "R", distances used in the discussion of intercolumnar charge recombination are also shown.

unsubstituted phthalocyanine. The actual "edge" corresponds, therefore, to a circle drawn close to the oxygen nuclei in the present alkoxy compounds.

The value of V_m for the PcOC5 compound, which was not investigated by SAXS, was interpolated from the straight line plot of V_m against n. D was derived from this using (3) and taking 3.4 Å for c.

Solid Phase. In the solid phase of the n-alkoxy derivatives the readily identifiable diffraction pattern indicative of hexagonal columnar packing is replaced by a more complex series of sharp lines.[56−58] In addition, the 3.4 Å reflection characteristic of horizontal stacking of the molecules is absent and is replaced by a reflection at approximately 4.2 Å. On the basis of these observations, it is concluded that, while a columnar structure remains, the molecules are now tilted with respect to the columnar axis, as illustrated at the right in Figure 2.

The X-ray patterns were initially indexed by van der Pol et al.[55,56] using an orthorhombic unit cell with $Z = 4$ molecules per unit cell. However, from the lattice parameters so derived, the density of PcOC6 is calculated to be 1.48 g/cm^3. This is

TABLE 2: Unit Cell Parameters Derived from Small Angle X-Ray Scattering (SAXS) Data[a]

			solid[e]			
compound	D_{max}[b]	mesophase[c] D	a	b	c	θ
PcOC5	29.3	(26.1)[d]	(49.4)[d]	(20.9)[d]	(4.1)[d]	(123)
PcOC6	31.5	27.6	54.0	21.6	4.07	123
PcOC7	33.7	28.6	55.9	23.2	4.02	123
PcOC8	35.8	30.3	56.3	23.5	4.17	120
PcOC9	38.0	31.4	57.7	24.7	4.19	120
PcOC10	40.2	32.5	59.4	25.0	4.22	117
PcOC11	42.4	33.9	61.9	26.0	4.30	120
PcOC12	44.6	35.2	(65.1)[d]	(26.9)[d]	(4.2)[d]	(120)
PcOC18[f]	57.7	41.2	78.4	31.0	4.16	120

[a] For a description of the parameters see Figure 2. For comparison, the maximum molecular diameter calculated assuming all-trans alkyl chains, D_{max}, is also given. All distances are in angstroms, and angles, in degrees. [b] $D_{max} = 14.8 + 2\cos(30°)(3.33 + 1.26(n-1))$. [c] SAXS at 200 °C (refs 55,56). [d] Interpolated. [e] Based on an oblique unit cell with $Z = 2$. [f] Own measurement.

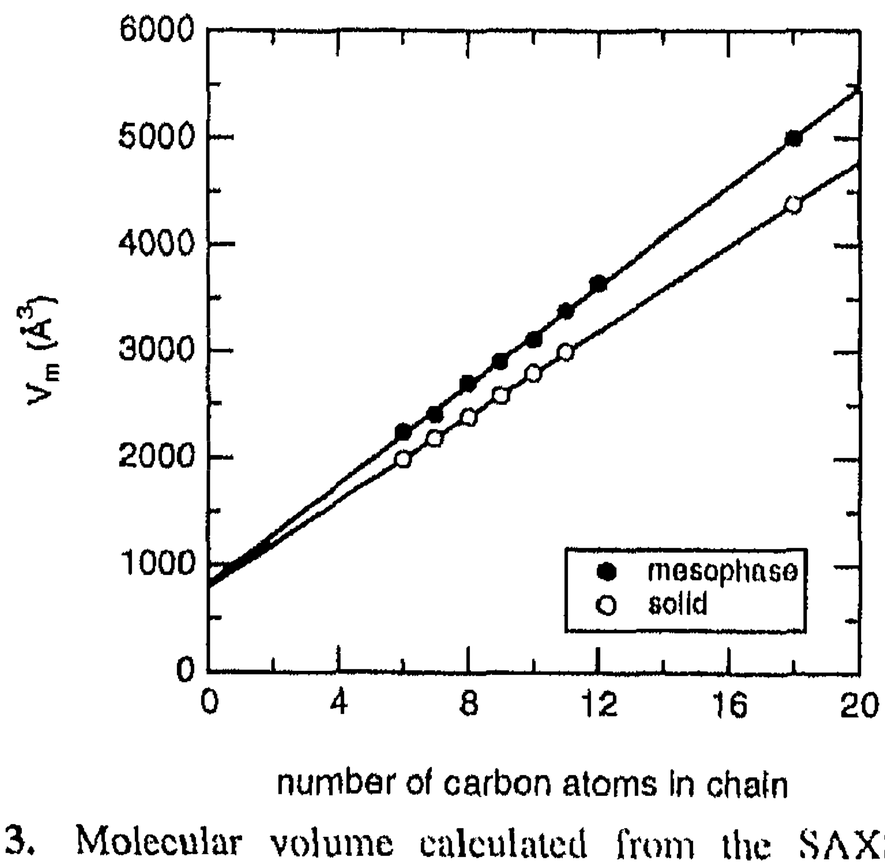

Figure 3. Molecular volume calculated from the SAXS lattice parameters as a function of the number of carbon atoms in the n-alkoxy chain.

even larger than the density of pure phthalocyanine (1.45 g/cm^3) and leads to an estimate of the density of the hydrocarbon region more than 1.5 times the *ca.* 0.9 g/cm^3 found for n-alkane solids. On finding that crystals of PcOC6 float on 1,2-dichloroethane (ϱ = 1.25 g/cm^3), we decided to reanalyze the available X-ray data, applying the restriction that the density calculated on the basis of the X-ray analysis should be equal to the actual density measured.

The densities of a selection of PcOCn solids were determined by flotation densimetry. This involves placing a few small

TABLE 3: Characteristics of the Saturated Hydrocarbon Barrier[a]

	mesophase			solid		
compound	R_{max}[b]	R_D[c]	$\varrho(Cn)_D$[d]	$\langle R_K \rangle$[e]	$\varrho(Cn)_K$[d]	$R_D/\langle R_K \rangle$
PcOC5	14.5	11.3	0.81	9.4		1.20
PcOC6	16.7	12.8	0.81	10.7	0.96	1.20
PcOC7	18.9	13.8	0.84	11.9		1.16
PcOC8	21.0	15.5	0.81	12.4		1.25
PcOC9	23.2	16.6	0.82	13.4	0.95	1.24
PcOC10	25.4	17.7	0.83	14.0		1.26
PcOC11	27.6	19.1	0.81	15.2		1.26
PcOC12	29.8	20.4	0.80	16.3	0.94	1.25
PcOC18	42.9	26.4	0.81	21.6	0.94	1.22

[a] Distances are in angstroms and are defined in Figure 2; densities are in g/cm^3. [b] $R_{max} = D_{max} - 14.8$. [c] $R_D = D - 14.8$. [d] Based on a PcH molecular volume of 587 Å^3, diameter = 14.8 Å (ref 66). [e] Using eq 11.

crystals of the material in a nondissolving liquid of lower density contained in a preweighed graduated cylinder. A liquid of density higher than that of the material of interest is then added until, after mixing, the crystals remain suspended, neither rising nor sinking. The total volume of liquid is then read; the cylinder plus contents, weighed. The density values determined in this way are listed in Table 1 as ϱ_K and are considered to be accurate to within a few percent. These values, together with interpolated densities for compounds not directly measured, were used in the reanalysis of the X-ray data. From these overall densities the density of the hydrocarbon regions can be estimated taking for phthalocyanine $\varrho = 1.45$ g/cm^3. These values are listed in Table 3 as $\varrho(Cn)_K$. They are only slightly larger than the densities of the corresponding solid *n*-alkanes.

In addition to fixing the density in the analysis of the SAXS data, the intracolumnar spacing, *c*, was taken to be equal to the alkyl chain length independent reflection at approximately 4.2 Å. The measured values of *c* are listed in Table 2.

For an orthorhombic unit cell with rectangular sides *a* and *b* one has

$$ab = \frac{ZM_w}{cN_{Av}} \times 10^{24} \text{ (Å}^2\text{)} \quad (5)$$

with all of the parameters on the right-hand side being known or measurable. This condition was used to interrelate the *a* and *b* values which were substituted into the relationship for the *hkl* reflections:[67]

$$d_{hkl} = \left[\frac{h^2}{a^2} + \frac{k^2}{b^2} + \frac{l^2}{c^2}\right]^{-0.5} \quad (6)$$

Using this approach, an orthorhombic unit cell was found to be incapable of indexing a significant number of the reflections observed whether $Z = 2$ or 4 was used.

The most successful indexing was found for an oblique unit cell with $Z = 2$.[57] The corresponding molecular arrangement is shown in Figure 2, with the unit cell parameters indicated. The condition relating the fit parameters used in this case was

$$ab \sin\theta = \frac{ZM_w}{cN_{Av}} \times 10^{24} \text{ (Å}^2\text{)} \quad (7)$$

The spacings are given by[67]

$$d_{hkl} = \left[\frac{\frac{h^2}{a^2} + \frac{k^2}{b^2} + \frac{2hk\cos\theta}{ab}}{\sin^2\theta} + \frac{l^2}{c^2}\right]^{-0.5} \quad (8)$$

A best overall fit to the most prominent x-ray reflections was obtained by varying *a* and the angle θ, which was taken initially to be 120°. The unit cell parameters derived are listed in Table 2.

The molecular volumes obtained for the solids, according to

$$V_m = abc(\sin\theta)Z \quad (9)$$

are plotted against *n* in Figure 3. The volume increment per methylene group is determined to be 24.9 Å^3, which is very close to the values of 25.4 and 26.2 Å^3 found for solid *n*-alkanes and *n*-alcohols.[65] The value of $V_m(0) = 797$ Å^3 found as intercept at $n = 0$ is only slightly smaller than the value found by extrapolation of the mesophase data. For a molecular thickness of 3.4 Å this corresponds to a diameter of 17.3 Å.

For PcOC5 and PcOC12 no SAXS data were available for the solid. The values of V_m were therefore interpolated from the straight line in Figure 3. The *a* and *b* distances were then derived from V_m using the values of *c* and θ given in Table 2 together with the average *a*/*b* ratio of 2.42 found for the other compounds.

In the solid phase there are two nearest neighbor intercolumnar distances, *a*/2 and *b*, as can be seen in Figure 2. Because of the tilt of the Pc units, the projection of the core along the columnar axis is ellipsoidal, with a long axis close to the Pc macrocycle diameter of 14.8 Å and a short axis of $14.8 \times 3.4/c$ Å. To obtain estimates of the edge-to-edge distances in the solid, R_{Ka} and R_{Kb}, we have taken the effective core diameter to be the average of the ellipsoidal axes;

$$R_{Ka} = 0.5[a - 14.8(1 + 3.4/c)] \quad (10a)$$

$$R_{Kb} = b - 7.4(1 + 3.4/c) \quad (10b)$$

For discussion of the distance dependence in the solid phase we use the average of these two values, denoted $\langle R_K \rangle$ in Table 3 and given by

$$\langle R_K \rangle = (R_{Ka} + R_{Kb})/2 = 0.25a + 0.5b - 7.4(1 + 3.4/c) \quad (11)$$

Experimental Section

The pulse-radiolysis time-resolved microwave conductivity, PR-TRMC, technique has been described previously.[68-70] The materials were contained in a microwave cell which consists of a piece of rectangular waveguide of cross section 7.1 × 3.55 mm^2 closed at one end with a metal plate. Approximately 200 mg of material was compressed into the cell using a close-fitting Teflon rod, and then the weight and length of the sample were measured. The temperature of the cell could be varied over the range −100 to +200 °C. When less material was available, use was made of a Perspex block with a rectangular-shaped cavity of 2 × 6 × 3 mm^3, which could be filled with approximately 25 mg of material. The Perspex block was then placed in the microwave cell. Using the Perspex block, the upper temperature was limited to 120 °C.

The samples were ionized by pulsed irradiation with 3 MeV electrons from a van de Graaff accelerator using pulse widths of 2−50 ns. The integrated beam charge per pulse, *Q* (in nC), was monitored routinely. The energy deposition was close to uniform throughout the sample[70] and equal to 0.58*Q* Gy (1 Gy = 1 J/kg), measured using thin-film radiochromic dosimeters (Far West Technology Nr92). A single 10 ns, 4 A pulse gave a total energy deposition of 23 Gy in the sample. Taking an average energy of 25 eV for the formation of one electron−

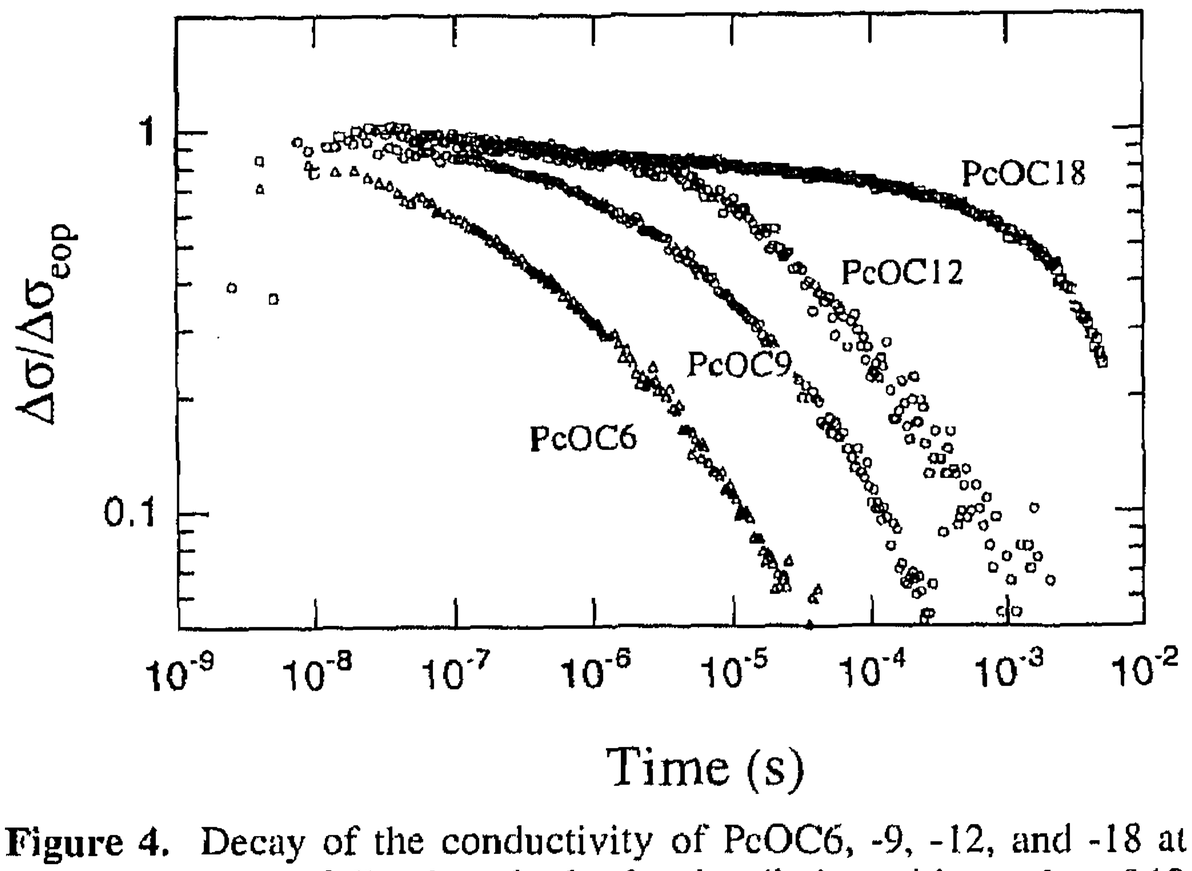

Figure 4. Decay of the conductivity of PcOC6, -9, -12, and -18 at room temperature following single-shot irradiation with a pulse of 10 ns duration and a dose of *ca.* 2×10^4 J/m^3.

hole pair,[71,72] this dose corresponds to the formation of approximately 6×10^{21} pairs/m^3, i.e. a concentration of *ca.* 10^{-5} molar.

Changes in the conductivity of a sample on pulsed irradiation were detected as changes in the microwave power reflected by the sample. Changes in the output of the microwave detector diode were monitored using either a Tektronix 7912 digitizer with a time resolution of 1 ns or a tandem combination of a Tektronix 2205 oscilloscope (7A13 plug-in) and a Sony/Tektronix RTD digitizer capable of monitoring data points from 10 ns to 10 ms on a pseudologarithmic time-base following a single radiation pulse.

For small changes, the change in reflected microwave power, ΔP, is directly proportional to the radiation-induced conductivity change, $\Delta\sigma$. Using computational procedures described previously, the absolute value of $\Delta\sigma$ can be determined.[69,73,74] The radiation-induced conductivity changes measured in the present study usually lay between 10^{-4} and 10^{-3} S/m. This is at least 8 orders of magnitude higher than estimated for the intrinsic conductivity due to charge carriers in unirradiated, pure materials.[75]

Results and Discussion

Readily measureable changes in conductivity are observed on pulsed irradiation of all of the octaalkoxyphthalocyanines studied, in both their solid and liquid crystalline phases. Characteristic PR-TRMC traces are shown in Figure 4 for PcOC*n* derivatives, with $n = 6$, 9, 12, and 18, at room temperature. The results show that mobile charge carriers are formed which have lifetimes considerably longer than the nanosecond pulse-lengths used.

The radiation-induced conductivity, $\Delta\sigma$, is related to the concentration of charge carrier pairs formed, N_p, and the sum of their mobilities, $\sum\mu = [\mu(+) + \mu(-)]$, by

$$\Delta\sigma = eN_p\sum\mu \tag{12}$$

The end-of-pulse conductivity, $\Delta\sigma_{eop}$, per unit energy absorbed by the sample, D (J/m^3), is given by[51]

$$\Delta\sigma_{eop}/D = W_{eop}\sum\mu/E_p \tag{13}$$

with E_p the average energy in electronvolts required to form one e^-h^+ pair and W_{eop} the probability that initially formed e^-h^+ pairs survive rapid (subnanosecond) geminate recombination and still exist at the end of the pulse.

By making estimates of E_p and W_{eop}, values of $\sum\mu$ as large as 10^{-5} m^2/(V s) have been determined for the present compounds, corresponding to intracolumnar jump times of a few hundred femtoseconds.[52] Very recently direct, time-of-flight mobility measurements on aligned samples of analogous mesomorphic triphenylene derivatives have yielded similar absolute mobility values and show similar trends at phase transitions,[76-78] thus providing support for the values determined by the present more indirect but more widely applicable PR-TRMC method.

In a previous publication[52] the main concern was with the effect of the nature of the peripheral chains and temperature on the magnitude of the end-of-pulse conductivity. For the same conditions of phase and temperature $\Delta\sigma_{eop}/D$ was, in fact, found to be relatively insensitive to the length of the peripheral alkyl chains for the *n*-alkoxy-Pc derivatives with $n = 5-18$.

The insensitivity of the end-of-pulse conductivity to the nature of the peripheral substituents is in complete contrast to the very marked effect of increasing chain length on the after-pulse decay, as shown by the transients in Figure 4. It is this dependence of the decay kinetics on the nature of the peripheral substituents and the physical conditions that is the subject of the present paper. We begin by considering the various processes which could be responsible for the decay of the conductivity following the pulse.

Conductivity Decay Mechanism. The gradual decrease in the radiation-induced conductivity with time following the pulse can result from either a decrease in the charge carrier mobilities due to localization at impurity or domain boundary sites or a decrease in the carrier concentration due to charge recombination. These possibilities can be represented generally by

$$\Delta\sigma(t) = eN_p(t)\sum\mu(t) \tag{14}$$

Because of the very large electron affinity, *ca.* 3 eV, and very low ionization potential, *ca.* 5 eV, of the phthalocyanine moiety in the solid state,[79] the number of organic compounds capable of functioning as competitive traps for electrons or holes is extremely limited. The columnar aggregation process would be expected to have a zone-refining effect which would allow only molecules with a closely similar molecular structure to be incorporated into a stack. The only likely candidates as impurity-trapping sites within the Pc core therefore would be metal derivatives of phthalocyanine with redox properties different from those of the metal-free compounds.

In view of the method of preparation of the compounds[55] the most likely impurity would be the CuPc derivative. Deliberate addition of percentage amounts of CuPcOC9 to PcOC9 was, however, found to have no significant effect on either the magnitude or decay kinetics of the radiation-induced conductivity transients. Since the electron affinity of CuPc is estimated to be 0.26 eV larger than H_2Pc while the ionization potentials are very similar,[79] the lack of effect of CuPc on the conductivity may indicate that it is the hole that is the major charge carrier. This would be in agreement with conclusions drawn for analogous mesomorphic triphenylene derivatives in time-of-flight studies.[76-78]

Physical sources of potential charge carrier trapping sites are domain or grain boundaries. In the present compounds the length of the integral columns within organized domains has been estimated[56,80] to be a few thousand Pc units or *ca.* 1 μm. The average time for a charge carrier to diffuse over the characteristic dimension of a domain, L, via one-dimensional,

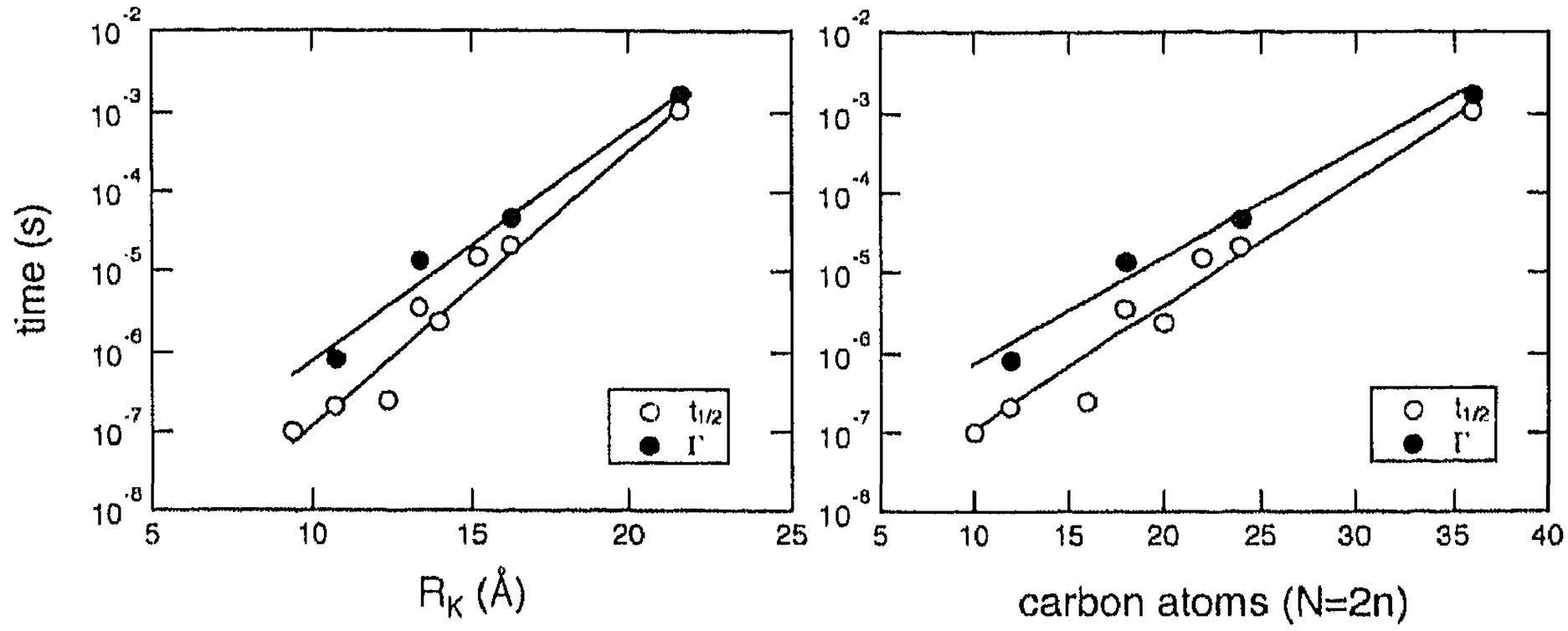

Figure 5. Open circles: the first half-lives of the conductivity transients at room temperature plotted as a function of the average nearest neighbor edge-to-edge distance $\langle R_K \rangle$ (left) and the total number of carbon atoms, $N = 2n$, in the alkyl chains forming the hydrocarbon barrier (right). Filled circles: similar plots using the $1/e$ decay time of the transients.

TABLE 4: Experimental First Half-Lives for the Radiation-Induced Conductivity Decay in *n*-Alkoxy-Pc Derivatives at Different Temperatures

	$t_{1/2}$ (s)					
compound	−100 °C	−50 °C	RT	T_{K-D} − 10 °C	T_{K-D} + 10 °C	200 °C
PcOC5			1.0×10^{-7}	1.1×10^{-6}	1.9×10^{-6}	
PcOC6	8.0×10^{-9}	2.5×10^{-8}	2.0×10^{-7}	1.0×10^{-6}	1.3×10^{-6}	4.0×10^{-7}
PcOC8			2.3×10^{-7}	7.1×10^{-7}	1.7×10^{-6}	
PcOC9	4.9×10^{-7}	1.4×10^{-6}	3.5×10^{-6}	7.1×10^{-6}	1.6×10^{-5}	4.6×10^{-6}
PcOC10			2.3×10^{-6}	3.2×10^{-6}	1.7×10^{-5}	
PcOC11			1.5×10^{-5}	2.2×10^{-5}	2.4×10^{-5}	
PcOC12	1.4×10^{-5}	1.5×10^{-5}	2.0×10^{-5}	5.6×10^{-5}	3.1×10^{-4}	5.6×10^{-5}
PcOC18	1.3×10^{-3}	1.9×10^{-3}	1.0×10^{-3}	6.3×10^{-4}	1.6×10^{-6}	1.1×10^{-6}

intracolumnar hopping is given by

$$t_{1/2} \approx t_j[L/d_j]^2 \qquad (15)$$

where t_j and d_j are the site-to-site jump time and jump distance. For PcOC*n* compounds at room temperature d_j is 4.2 Å and t_j has been estimated to be 0.14 ps.[52] The time required to diffuse over a distance of *ca.* 1 μm is therefore on the order of 1 μs. The fact that lifetimes of mobile carriers up to milliseconds are observed, as shown by the data in Figure 4, indicates that domain boundaries or "column ends" apparently do not, in fact, function as trapping sites in the present materials.

A particularly strong piece of evidence against the conductivity decay being controlled by charge carrier trapping at either impurity or domain boundary sites is the very pronounced and consistent increase in lifetime of the transients with increasing alkyl chain length. There is no reason to expect that impurity levels or domain sizes would depend as much or as consistently on the length of the peripheral chain as would be required to explain these observations.

If the first half-lives of the transients shown in Table 4, together with data for other compounds in the *n*-alkoxy series, are plotted logarithmically against the total number of carbon atoms separating the columns, i.e. $N = 2n$, then a reasonably good linear dependence is found, as shown in Figure 5. The exponential dependence of the half-life on distance indicated, i.e.

$$t_{1/2} = \tau_N \exp[\beta_N N] \qquad (16)$$

suggests very strongly that the conductivity decay is, in fact, due to charge recombination controlled by electron transfer through the hydrocarbon mantle surrounding the phthalocyanine cores.

The decay kinetics are found to be unaffected by the concentration of charge carriers formed when this is varied from approximately 2 to 20 μM by increasing the dose in the pulse. This is found to be the case even for the PcOC18 compound, for which the after-pulse decay extends into the millisecond region. Recombination does not therefore occur "homogeneously", i.e. between positive and negative charge carriers formed in different regions of the sample, since then the decay rate should increase with increasing concentration. Rather, recombination must take place between electrons and holes which remain Coulomb-correlated throughout their lifetime.

The physical model which we find best describes the experimental observations is illustrated schematically in Figure 6A,B. In this model the charge carriers responsible for the radiation-induced conductivity originate as electron-hole pairs formed by ionization events within the hydrocarbon tail regions.[52] During the course of their mutual diffusional motion and prior to their geminate recombination, a fraction of these pairs undergo electron and hole scavenging by the Pc cores of different stacks. This is illustrated in Figure 6A.

The elongated lifetime of the core-localized carriers results from the fact that the electron affinity of phthalocyanine is much larger than that of the alkane medium, 3 eV[79] versus close to 0 eV,[81] and the Pc ionization potential is much lower, 5 eV[79] versus *ca.* 8 eV.[82,83] The barriers to intercolumnar electron and hole transfer will therefore both be approximately 3 eV. Charge recombination can then only occur via long-distance tunneling through the hydrocarbon mantle, as illustrated schematically in Figure 6B.

The necessity of a substantial, insulating hydrocarbon barrier between the macrocyclic stacks in order to observe long-lived mobile charge carriers at all, is demonstrated by the complete absence of an after-pulse conductivity for the octamethoxy derivative.[49] An electron and hole localized on the same stack or contingent stacks apparently recombine extremely rapidly, i.e. on a time scale much shorter than nanoseconds.

Decay Kinetics. The decay of the conductivity transients in

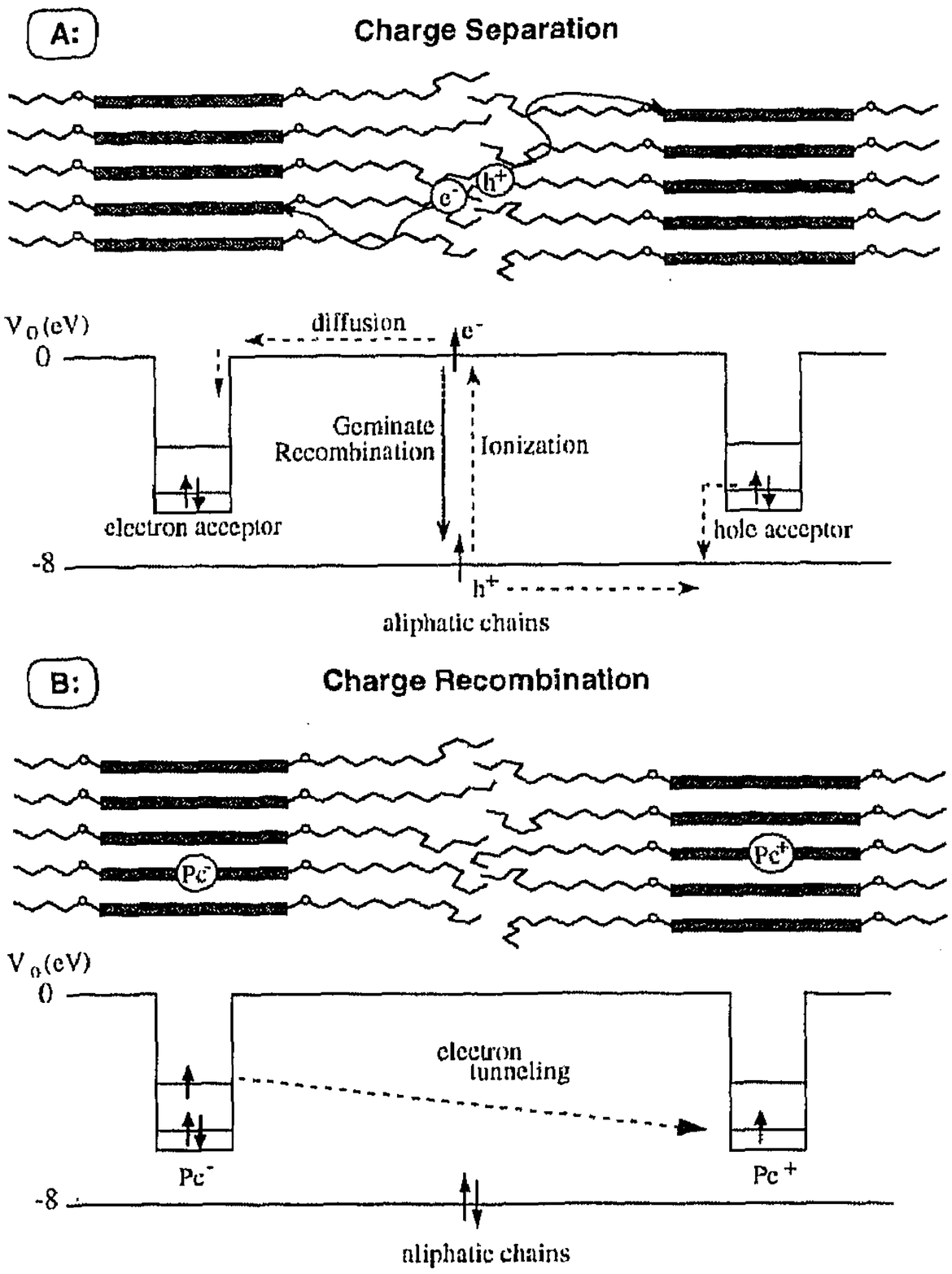

Figure 6. (A) Schematic representations of the processes involved in the formation of separated electron−hole pairs. (B) Schematic representations of the charge recombination process via long-distance electron transfer through the hydrocarbon mantle surrounding the phthalocyanine cores.

the present materials deviates considerably from that expected for a process with a time-independent rate coefficient, i.e. monoexpoential. We have investigated the applicability of a form of kinetics first introduced empirically by Kohlrausch[84] which has been found to provide a description of disperse kinetics in a large variety of mainly solid state systems.[85,86] The general form of the time evolution of the concentration in this approach is given by

$$N(t) = N(0)\exp[-(t/\Gamma)^{\alpha}] \qquad (17)$$

For $\alpha = 1$, eq 17 corresponds to a monoexponential decay with a time-independent rate constant $1/\Gamma$. For $\alpha < 1$ the rate effectively decreases with time, resulting in the disperse decay kinetics characteristic of the present systems. It should be pointed out that the logarithmic time base use in Figure 4, which is necessary to display all of the data in one figure, does not provide a good illustration of the pronounced tailing in the decays which is apparent on a linear time scale.[49]

A time dependence of the form of eq 17 is found to provide a good description of many of the conductivity transients observed in the present work. An example is shown in Figure 7 for the conductivity in PcOC9 at room temperature. The data in this case are plotted as $\ln[\Delta\sigma(t)/\Delta\sigma(0)]$ against t^{α} for different values of α. A "best-fit" value of α should then result in good straight-line behavior within the time-window of the transient, which was 10 ns to 0.5 ms. As can be seen, a value of α close to 0.25 does in fact result in good linearization of the data.

The ability of eq 17 to provide an empirical fit to the data is further illustrated by the calculated lines drawn through the conductivity transients in Figures 8 and 9. As can be seen, in

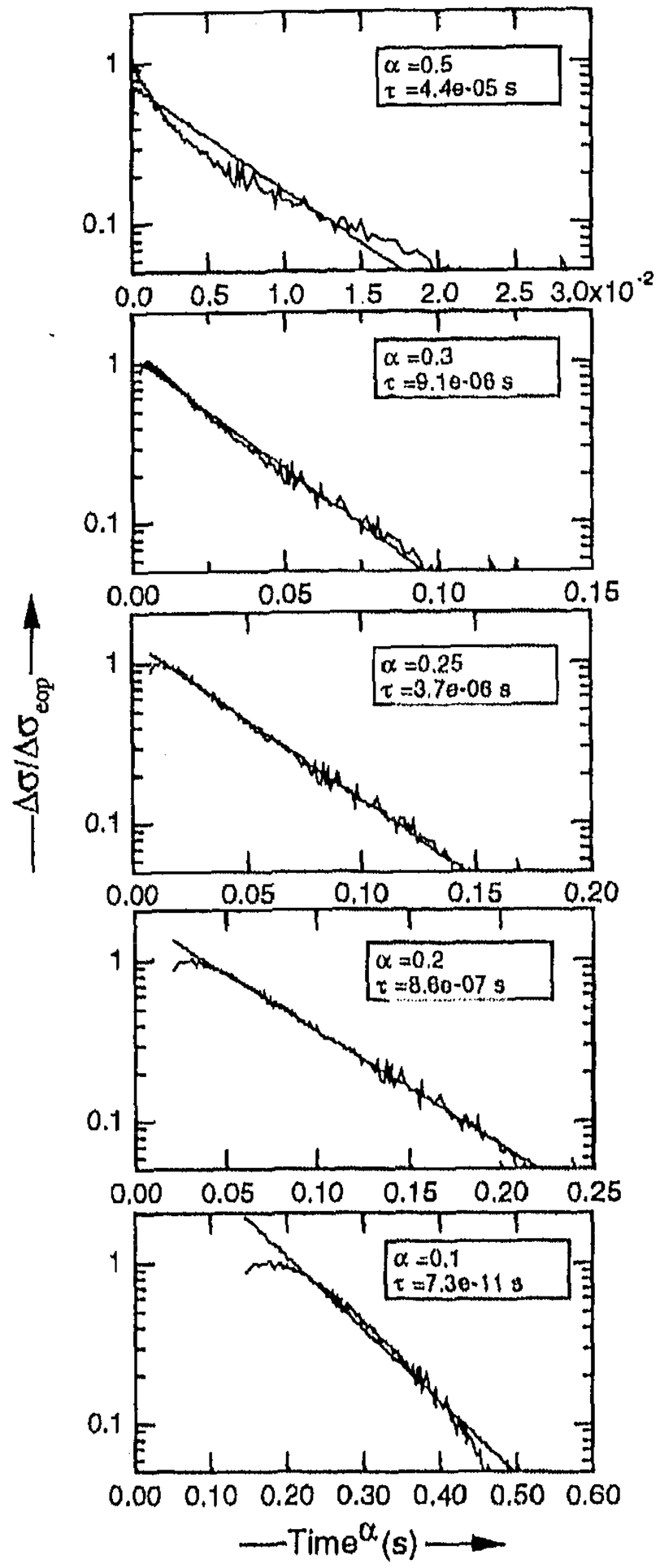

Figure 7. Examples of Kohlrausch fits to the conductivity transient for PcOC9 at room temperature with α varied from 0.1 to 0.5.

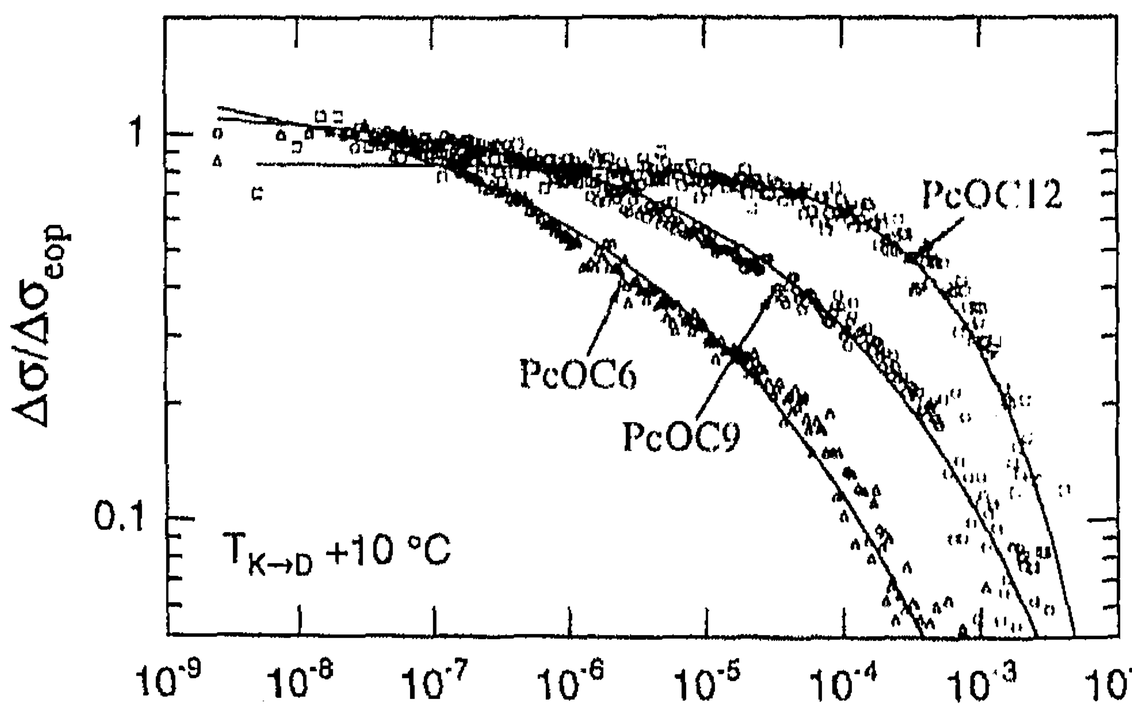

Figure 8. Decay of the radiation-induced conductivity of PcOC6, -9, and -12 at 10° above the K → D transition temperature following single-shot irradiation with a pulse of 10 ns duration and a dose of *ca.* 2×10^4 J/m^3. The lines were calculated using the Kohlrausch expression, eq 17.

certain cases a reasonably good fit can be obtained over the complete transient time scales. However, this is not true in all cases. Because of this, in subsequent sections we have chosen to discuss the characteristic time scale of the conductivity decays in terms of the phenomenological parameter, the first half-life, $t_{1/2}$, rather than the lifetime parameter, Γ, in the Kohlrausch

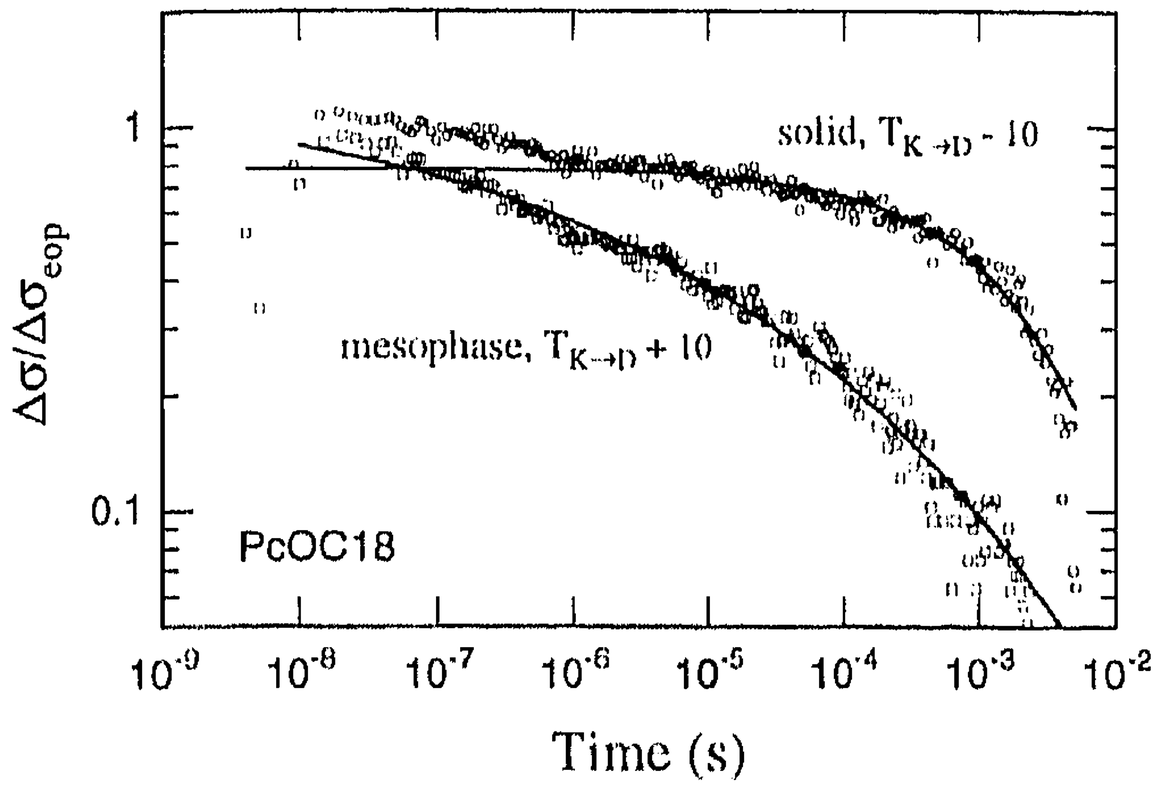

Figure 9. Effect of the K → D transition on the decay kinetics of the radiation-induced conductivity transient in PcOC18. The lines were calculated using the Kohlrausch expression, eq 17.

expression. In what follows, however, we discuss the consequences of this for the eventual values of the exponential distance parameters determined from the data.

As can be seen from (17), Γ is the time at which the signal has decayed to $1/e$ of its initial value. This parameter will always be somewhat longer than the half-lifetime to which it is related by the expression

$$\Gamma = t_{1/2}[\ln 2]^{1/\alpha} \tag{18}$$

Thus for $\alpha = 1$, 0.5, and 0.2, Γ will be a factor of 1.44, 2.08, and 6.25 longer than $t_{1/2}$. If the degree of dispersion in the kinetics, i.e. α, is constant, then the quantitative conclusions drawn in the following sections about the influence of distance and temperature on the time scale of the decay kinetics will be independent of whether $t_{1/2}$ or Γ is used since the ratio between the two is then constant. If, however, α varies with distance or temperature, this will no longer be the case.

For the PcOCn compounds, α does, in fact, increase with increasing chain length, with values of 0.25, 0.25, 0.45, and 0.70 for $n = 6$, 9, 12, and 18 at room temperature. To illustrate the effects of differences in dispersion, we have plotted in Figure 5 the values of Γ in addition to $t_{1/2}$. The β_N parameter derived from the slope of the ln[Γ] against the N plot is 0.31 compared with 0.36 determined using $t_{1/2}$. In general, lower values of the β parameter would be derived using Γ as the characteristic time because of the larger dispersion for the shorter chain compounds.

The magnitude of the dispersion parameter α may provide an additional insight into the details of the processes underlying the dynamics of long-distance charge recombination in the present type of complex molecular system. The values determined from best fits to the kinetic data for PcOCn with $n = 6$, 9, 12, and 18 are given as a function of temperature in Figure 10. As can be seen, α remains fairly constant for the three shortest chain compounds with even at the K → D transition temperature only a relatively small increase or decrease being observed. For PcOC18, however, the transition is accompanied by a dramatic decrease in α from 0.6 to 0.2. As will be discussed later, we associate this change with a change in the mechanism of intercolumnar charge recombination from electron tunneling to molecular ion diffusion between columns.

The underlying reason for the disperse nature of the kinetics is not yet known. The fact that it is larger for the shortest chain compounds in the solid phase would suggest that it is related in some way to a variability in the intercolumnar distance or in the nature of the chain-end regions, which would tend to play a more important role for the shorter distances. We have initiated a theoretical study into the possible sources of the dispersion in the recombination kinetics in the present materials and hope in the future to be able to discuss this aspect in greater depth.

It is perhaps worth noting that we have found disperse decay kinetics to be characteristic of all of the complex molecular solids that we have studied. The necessary use of "multiexponential" fits to decays in biological systems may also reflect a degree of dispersion in the kinetics rather than separate kinetic processes or species, as is often assumed.

TABLE 5: β and τ Parameters Characterizing the Distance Dependence of the Experimental $t_{1/2}$ Data According to Eqs 16 and 17 at Different Temperatures[a]

T (°C)	τ_N (s)	β_N	τ_R (s)	β_R (Å^{-1})
−100	4.5×10^{-11}	0.48	1.6×10^{-13}	1.08
−50	2.0×10^{-10}	0.45	1.1×10^{-12}	1.00
RT	2.9×10^{-9}	0.36	4.3×10^{-11}	0.79
$T_{K\rightarrow D} - 10$	1.4×10^{-8}	0.32	1.8×10^{-9}	0.59
$T_{K\rightarrow D} + 10$	1.0×10^{-8}	0.40	4.0×10^{-10}	0.63
200	2.9×10^{-9}	0.41	1.0×10^{-10}	0.65

[a] The nearest neighbor edge-to-edge distances $\langle R_K \rangle$ and R_D given in Table 3 were used for the solid and mesophase, respectively.

Distance Dependence in the Crystalline Solid. As mentioned in a previous section and shown in Figure 5, the first half-lives of the radiation-induced conductivity transients for the PcOCn compounds display a close to exponential dependence on the number of carbon atoms in the peripheral alkyl chains separating two Pc stacks. Because of the discoid shape of the molecules and the close to constant density of the hydrocarbon mantle, the intercolumnar distance is not, however, a linear function of n. Therefore, there is not a constant factor relating β_N to the exponential distance parameter β_R, as given by (19).

$$t_{1/2} = \tau_R \exp[\beta_R R] \tag{19}$$

Separate plots of $t_{1/2}$ against the actual intercolumnar distance measured are therefore required in order to determine β_R.

It is worth pointing out that in previous experimental studies of electron transfer through n-alkane barriers using two-dimensional alkyl chain surfactant layers no measurement of the actual width of the hydrocarbon barrier between the electron transfer sites was made.[38-43] To estimate the distance and hence obtain a value for β_R, certain assumptions about the structure of the barrier had to be made. These include the tilt angle of the chains with respect to the supporting surface, the extent of intermeshing at chain ends, and the frequency of the occurrence of other than all-trans chain configurations.

In Figure 9 $t_{1/2}$ values for the present compounds are plotted against the measured edge-to-edge distance between phthalocyanine stacks, $\langle R_K \rangle$, at various temperatures. Good agreement with an exponential distance dependence, as represented by (19), is found at all temperatures. The values of β_R together with β_N and the corresponding values of τ_R and τ_N are listed in Table 5.

An aspect of the results which is particularly surprising is the pronounced temperature dependence of the β_R values in the solid phase. This will be discussed in more detail below after first considering two factors which could influence the absolute value of β_R at a given temperature.

The first of these has been mentioned in the previous section and concerns the fact that the functional time dependence of the conductivity decay is different for different compounds. This is shown in Figure 10 by the different α values obtained using

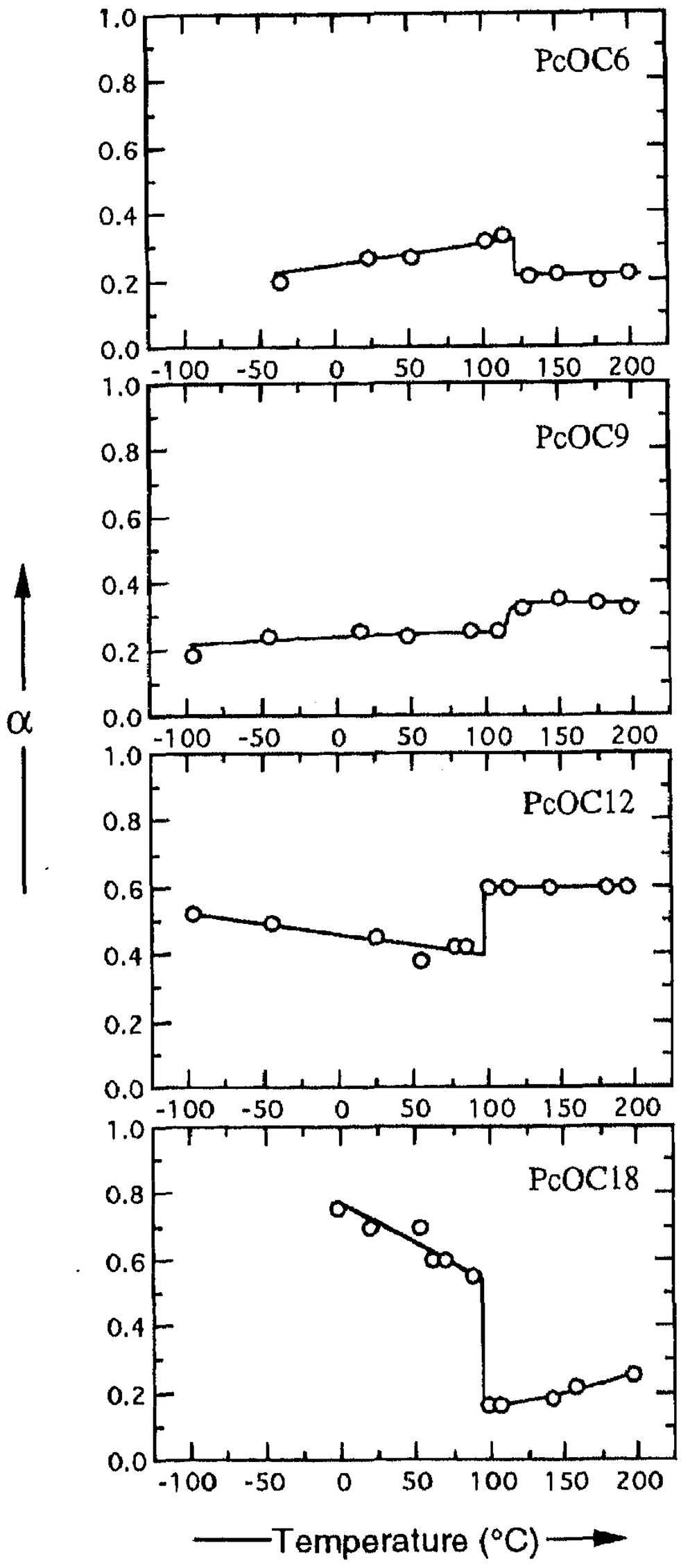

Figure 10. Dispersion parameter α in the Kohlrausch expression as a function of temperature for PcOC6, -9, -12, and -18.

the disperse kinetics relationship (17). Because α increases with increasing chain length, the result of plotting Γ against distance instead of $t_{1/2}$ is to decrease the value of β. This is illustrated for data at room temperature in Figure 5. The decrease in β_N is from 0.36 to 0.31 and for β_R from 0.79 to 0.67 Å^{-1}, i.e. approximately 15% for both parameters. Since α is only weakly dependent on temperature, as shown in Figure 10, the decrease by 15% found at room temperature will also be a good approximation at other temperatures.

The second factor which can influence the estimate of β_R from the experimental data (but not β_N!) is the choice of the path along which electron transfer actually occurs. For example by plotting the decay time against $\langle R_K \rangle$ in Figures 5 and 11, the implicit assumption is made that electron transfer occurs preferentially over the shortest edge-to-edge distance between the columns. Current "through-bond", "superexchange", and "optimal pathway" approaches to long-distance electron transfer, however, consider the detailed structure of the medium forming the barrier. On that basis, the most favored pathway would probably be chosen to lie along the direction of the alkyl chains in the plane of the molecules since that would minimize van der Waals gaps and maximize all-trans C—C bond configurations.

As can be seen in Figure 2, if electron transfer does occur preferentially in the plane of the molecules rather than perpendicular to the columnar axis, then the relevant distance is not $\langle R_K \rangle$ but rather a distance which we denote R_{KD}, similar to the distance R_D in the mesophase, where the molecules are horizontally stacked. In Table 3 the ratio of R_D determined in the mesophase to $\langle R_K \rangle$ in the solid is listed and is seen to be independent of alkyl chain length, with an average value of 1.23. Because of the *ca.* 12% higher density of the hydrocarbon mantle in the solid phase, R_{KD} will be smaller than R_D by approximately 6% and, therefore, a constant factor of 1.16 larger than $\langle R_K \rangle$. Using R_{KD} instead of $\langle R_K \rangle$ in plots such as those in Figures 5 and 11 would therefore result in β_R values a factor of 1.16 lower than the values listed in Table 5 for the solid phase. The β_N values and the β_R values in the mesophase given in Table 5 are of course unaffected by this preferred pathway problem.

Both of the factors discussed above would result in a decrease in the value of β_R compared with those given in Table 5. The combined effect of using Γ from eq 17 for the characteristic time of intercolumnar recombination rather than $t_{1/2}$ and the edge-to-edge distance in the plane of the molecules rather than $\langle R_K \rangle$ would be to decrease the β_R values for the solid phase by a factor of 1.36 from 0.79 to 0.58 Å^{-1} at room temperature and from 1.08 to 0.79 Å^{-1} at −100 °C.

Temperature Dependence in the Crystalline Solid. The decrease in β_R with increasing temperature in the solid phase, shown in Figure 11 and Table 5, results from an increase in $t_{1/2}$ (*decrease* in the decay rate) with increasing temperature, with the effect increasing with decreasing alkyl chain length. The recombination process would therefore appear to have a negative energy of thermal activation. This is illustrated more clearly in Figure 12, where the half-lives in the solid phase are plotted as $\log(t_{1/2})$ versus $1/T$, for $n = 6$, 9, 12, and 18. The temperature dependence is seen to be particularly strong for PcOC6, with $t_{1/2}$ increasing by close to 2 orders of magnitude on going from −100 to +100 °C. For PcOC9 and PcOC12 the increases are less dramatic, by factors of approximately 10 and 4, respectively, over the same temperature range, and for the PcOC18 compound, no tendency to either increase or decrease with temperature can be discerned.

In general the results tend toward a constant plateau value of $t_{1/2}$ at the lowest temperatures, with a thermally activated increase at elevated temperatures. The lines drawn through the data points in Figure 10 were calculated using the empirical expression

$$t_{1/2} = \tau_0 + \tau_A \exp(-E_A/k_B T) \qquad (20)$$

The values of the parameters used are listed in Table 6. As can be seen, the limiting low temperature half-life, τ_0, increases from 7 ns for PcOC6 to 1.3 ms for PcOC18, more than 5 orders of magnitude. When the τ_0 values are plotted semilogarithmically against $\langle R_K \rangle$, the β_R value found is 1.10 Å^{-1}, which is only slightly larger than the value of 1.08 Å^{-1} determined from the $t_{1/2}$ data at −100 °C.

A decrease in the rate of electron transfer with increasing temperature is theoretically possible for highly exoergic ("inverted region") electron transfer processes, as in the present case, for which charge recombination is approximately 2 eV exoergic. The effect would, however, be expected to be quite mild.[87,88] For example, on the basis of the semiclassical equation for electron transfer, eq 21,[89,90] the maximum inverse temperature

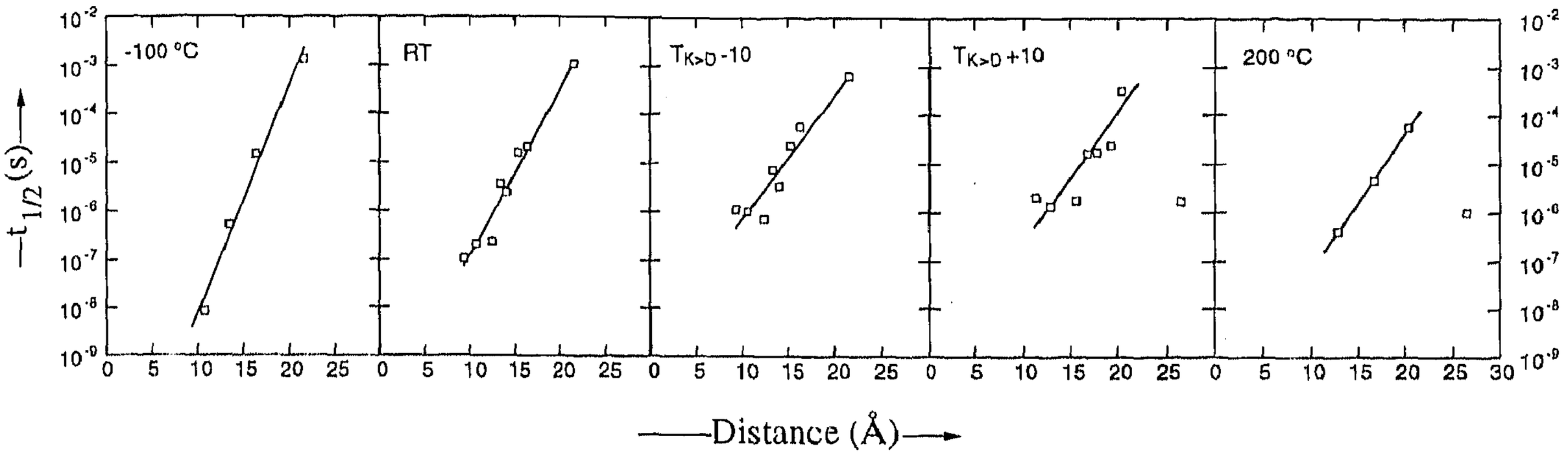

Figure 11. Half-life of the conductivity transient plotted against the nearest neighbor edge-to-edge intercore distance ($\langle R_K \rangle$ in the solid and R_D in the mesophase) at different temperatures.

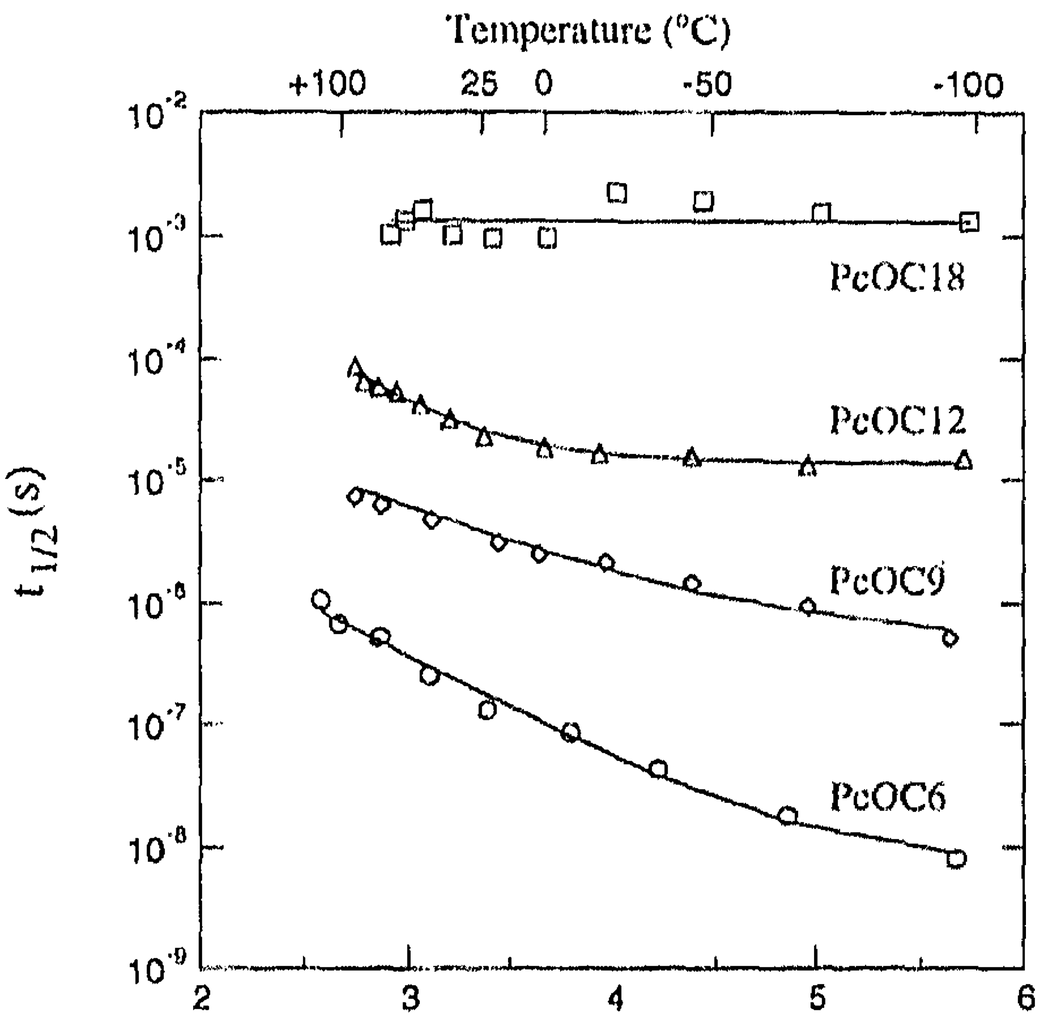

Figure 12. Arrhenius type plots of the half-life of the conductivity decays following pulsed irradiation of PCOC6, -9, -12, and -18 in the solid phase.

TABLE 6: Activation Energies and Preexponential Factors Yielding the Solid Lines in Figure 12 According to Eq 20

compound	τ_0 (s)	τ_A (s)	E_A (eV)
PcOC6	7.0×10^{-9}	1.4×10^{-4}	0.17
PcOC9	5.0×10^{-7}	5.0×10^{-4}	0.13
PcOC12	1.3×10^{-5}	0.1	0.23
PcOC18	1.3×10^{-3}		

dependence predicted would be $1/T^{0.5}$

$$k_{ET} = \frac{4\pi^2}{h} H_{AB}{}^2 \frac{\exp[-(\Delta G_{ET} + L)^2/4Lk_BT\chi]}{(4\pi Lk_BT\chi)^{0.5}} \quad (21a)$$

$$\chi = (h\nu/2k_BT)\coth(h\nu/2k_BT) \quad (21b)$$

In (21), H_{AB} is the matrix element describing the electronic coupling between the initial and final states, ΔG_{ET} is the free energy change involved in the transition, L is the reorganization energy, and ν is the frequency of the vibrational mode which most strongly couples to the electron transfer process. While more advanced theoretical treatments have been proposed, none would predict such a strongly negatively activated process as observed in the present work for the PcOC6 or PcOC9 compounds.

Experimental studies of highly exoergic, long-distance electron transfer in compounds with barriers consisting of rigid hydrocarbon bridges[5,91,92] have shown the rates to be close to independent of temperature. The rates of certain electron transfer processes in biological systems have been found to decrease somewhat with increasing temperature.[93-98] It has been proposed that this effect may be due to a decrease in density of the protein matrix with increasing temperature, resulting in an increase in the distance over which transfer must occur and, hence, a reduction in rate.[99] Jortner,[7] however, has estimated that for a distance of 20 Å and $\beta_R = 1$ Å^{-1} the decrease in rate due to thermal expansion would be at most approximately a factor of 2 on going from −120 °C to room temperature. Much larger effects are observed in the present materials. In addition, such a thermal expansion effect would be expected to be largest for the longest alkyl chain material, whereas the reverse is, in fact, found to be the case.

We conclude that the pronounced negative activation of the rate of recombination found for the present compounds is in some way related to conformational changes or fluctuations which occur at elevated temperatures within the hydrocarbon barrier and which result in a decrease in the overall electronic coupling between initial and final states.

The temperature dependence of the lifetime, as represented by (20), suggests that there are two processes operative, one of which is temperature independent and another which increases in prominence with increasing temperature and has a strong negative influence on the rate of electron transfer. A possible physical explanation would be if the barrier to electron transfer in fact consists of two regions: a strong coupling region, which would on its own result in rapid, temperature-independent electron transfer with rate k_s, and a weak coupling region with a much lower transfer rate, k_w. If the two regions act in series, then the net electron transfer rate is given by

$$1/k_{ET} = 1/k_s + 1/k_w \quad (22)$$

or in terms of the characteristic times,

$$\tau_{ET} = \tau_s + \tau_w \quad (23)$$

The slowest rate then acts as a bottleneck to the overall reaction. If the influence of the weak coupling region in some way increases with increasing temperature, then this could result in a decrease in the overall rate and hence an effective negative energy of activation.

The observation that the negative temperature dependence is most pronounced for the shortest alkyl chains suggests that the weak coupling is associated with the interfacial region between the chain ends since this will play a proportionately larger role the shorter the chain. In Figure 13 a schematic representation of the hydrocarbon region between two phthalocyanine stacks

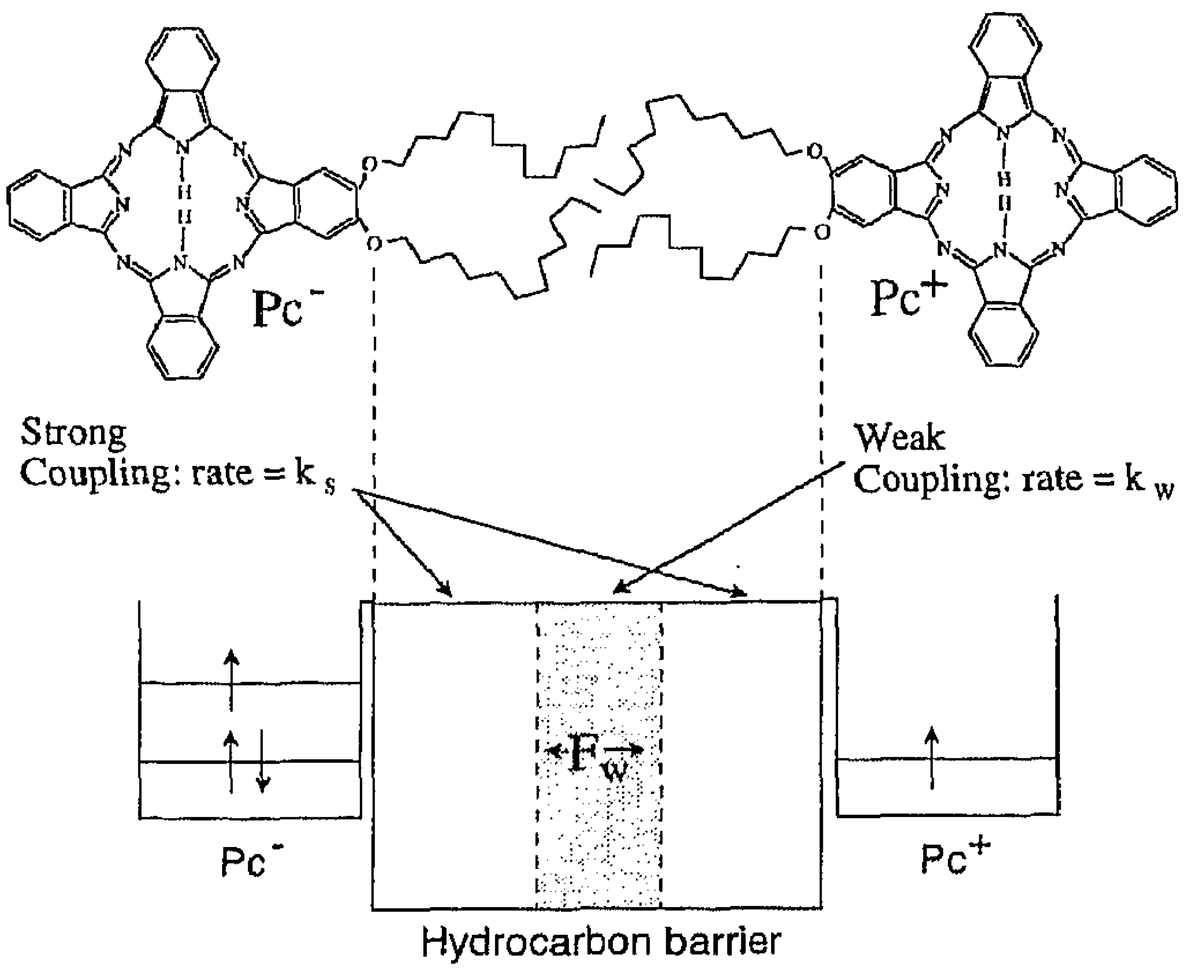

Figure 13. Schematic representation of the complex barrier to electron transfer with a strong coupling region close to the macrocyclic cores and a weak coupling region caused by conformational fluctuations ("premelting") in the interfacial barrier region.

is shown. We associate the strong coupling region within the barrier with all-trans chain configurations, which will probably dominate close to the macrocycle. The weak coupling region is associated with gauche kinks and van der Waals contacts, which will be most prevalent in the interfacial region.

The lack of perfect antiperiplanar ("all-trans") order in the chains is indicated by the SAXS data in Table 2, which show that the intercolumnar distance is much shorter than the diameter of a molecule with a fully outstretched, all-trans chain geometry even in the mesophase, where the molecules are horizontally stacked. The fact that the density calculated for the hydrocarbon region is the same as that for solid alkanes despite the radial geometry of the tails is also difficult to explain without the occurrence of gauche configurations and/or intermeshing between opposing chain ends.

It has been shown in NMR experiments on this type of compound that motion in the alkyl chains occurs even in the solid phase and that motional freedom begins at the chain extremities and gradually progresses toward the macrocycle end as the temperature increases.[100,101] This may be seen as a form of outside-in premelting within the barrier. Such premelting effects have also been observed by NMR, Raman, and infrared spectroscopy to occur even in *n*-alkane crystals which enter a rotator phase prior to melting.[102,103] In this phase, according to ref 102, "...the *n*-alkane chains start to perform uncorrelated large amplitude reorientation as well as translational motions...the molecules take up conformation defects located at the end of the chains...while their central parts remain in an almost fully extended "trans" conformation." Interestingly the interlaminar gap between end methyl groups is found to increase in the rotator phase.

At low enough temperatures all motion will be frozen and a constant, temperature-independent rate of electron transfer would be expected, as is found. We therefore associate the values of τ_0 with a conformationally completely rigid, crystalline hydrocarbon barrier. The barrier will, of course, still contain van der Waals gaps and quite probably frozen-in gauche kinks. It is not yet clear whether the negative effect of temperature on electron transfer is a static effect, due to an increase in the presence of "structural imperfections" in the interface region, or a dynamic effect, resulting from rapid conformational fluctuations in the structure. We tend to favor the latter explanation.

In terms of the premelting model proposed the hydrocarbon barrier is divided into a "crystalline solid" component with a (close to) temperature-independent lifetime for electron transfer, τ_s, associated with τ_0 in (20), and a "quasi-liquid" lifetime component, the contribution of which is thermally activated and gives rise to the second term on the right of eq 20. We accordingly associate the activation energies in Table 6 with the premelting process. The 0.1−0.2 eV range of E_A values is similar to that for the activation barriers of conformational changes in σ-bonded chains.

On the basis of the above, the limiting β_R value of 1.1 Å^{-1} obtained at low temperatures can be associated with a "completely frozen" (if not conformationally perfect) hydrocarbon barrier for all compounds. The values at elevated temperatures in the solid, however, refer to mixed media barriers in which electron transfer is controlled in part by the molecular structure and in part by conformational fluctuations with the relative importance depending on the chain length. Because the relative importance of the weak coupling component is larger for shorter chains, the values of β_R found at elevated temperatures in the solid phase are artificially low.

The Solid to Liquid Crystal Transition. At the solid to mesophase transition the hydrocarbon mantle becomes completely molten, as evidenced by several observations: (i) a large change in enthalpy is observed in DSC measurements, as shown in Table 1; (ii) X-ray diffraction studies show the density of the alkane region to decrease from 0.95 to 0.82 g/cm^3 (a value similar to that for liquid alkanes); (iii) the *ca.* 4.6 Å X-ray reflection characteristic of alkane chain packing becomes very diffuse;[56] (iv) ^{13}C NMR spectra become sharp and indicate rapid motion at all positions in the alkane chain;[100] (v) the dielectric loss suddenly increases[104−106] due to motional freedom even at the dipolar ether linkages.

While the hydrocarbon mantle takes on the properties of an isotropic liquid, the phthalocyanine macrocycles remain columnarly stacked and the intercolumnar spacing remains well-defined in SAXS diffraction patterns.[56,57] One difference in the mesophase is that the Pc units are stacked horizontally rather than tilted, resulting in hexagonal packing of the columns and a singular intercolumnar distance, as shown in Figure 2. The edge-to-edge distance between neighboring phthalocyanine stacks, R_D, is listed in Table 3 and is seen to vary from 11.3 Å for PcOC5 to 26.4 Å for PcOC18.

In Figure 8 are shown conductivity transients taken 10° above the K → D transition temperatures of the PcOC6, -9, and -12 compounds. A marked increase in the time scale of the decay with increasing chain length, similar to that found for the solid phase at room temperature, is apparent. We conclude, therefore, that the decay of the conductivity in the mesophase of these compounds is also controlled mainly by long-distance electron transfer through the (now liquid) hydrocarbon mantle. The time scale of the decay is, in general, longer than found in the solid just below the transition temperature. These results will be discussed in more detail after first considering the "anomalous" behavior of the PcOC18 compound.

The conductivity transients for PcOC18 taken at 10° above the phase transition temperature are shown in Figure 9. In contrast to the shorter chain compounds, the decay is found to be very much *faster* in the mesophase than in the solid, with $t_{1/2}$ actually decreasing by 3 orders of magnitude. The decay is, in fact, even faster than found in the mesophase of PcOC12. As pointed out in a previous section, a marked decrease in the kinetic dispersion parameter α from 0.6 to 0.2 is found to accompany this dramatic decrease in lifetime at the phase

transition, as shown in Figure 10, whereas only relatively small changes in α are found for the shorter chain compounds.

The anomalous behavior of PcOC18 cannot be attributed to a completely different mesophase structure since the SAXS pattern still displays the characteristics of horizontal columnar stacking of the Pc moieties and hexagonal packing of the columns. The compound is however found to have a very much lower viscosity in the mesophase than the shorter chain compounds and actually flows at *ca.* 100 °C. This is in agreement with the much lower clearing temperature of PcOC18: 247 °C compared with >300 °C for the other *n*-alkoxy derivatives. An anomalously high fluidity of the polysiloxane derivative of PcOC18 at 90 °C has also been reported.[107] We conclude that charge recombination occurs in the mesophase of PcOC18 preferentially by intercolumnar molecular ion diffusion rather than by intercolumnar electron tunneling due to the very low viscosity.

The average time scale of two-dimensional intercolumnar diffusion will be given approximately by the relationship

$$\tau_D \approx D^2/4\delta \qquad (24)$$

where D is the intercolumnar distance and δ the diffusion coefficient. Taking $D = 42$ Å for the PcOC18 compound, the value of δ required to result in a microsecond time scale for intercolumnar molecular diffusion is found to be 4×10^{-12} m^2/s. Intercolumnar molecular diffusion has been studied by NMR in the mesophase of analogous triphenylene derivatives.[108] Two-dimensional diffusion coefficients on the order of 5×10^{-11} m^2/s were found. The larger diffusion coefficient for the triphenylenes is in accordance with the much lower clearing temperatures of *ca.* 100 °C for these compounds, indicating a weaker columnar cohesion of the macrocycles, as might be expected on the basis of the much smaller size of the triphenylene core.

The shorter chain PcOC*n* derivatives have much higher clearing temperature and do not display the low-viscosity flow characteristics of PcOC18 in their mesophase. We conclude that intermolecular diffusion is very much slower for these materials and that charge recombination therefore occurs mainly via long-distance intercolumnar electron transfer, as would be suggested by the chain length dependence shown in Figure 8.

The effect of the solid to mesophase transition on the half-life of the conductivity decay for PcOC6, -9, and -12 is shown in Figure 14. An increase in $t_{1/2}$ is observed for all three compounds, although this is marginal for the PcOC6 compound. The effects are, in general, much less pronounced that might have been expected intuitively for such a dramatic change in the nature of the barrier. We conclude that the change from a rigid solid to a liquid medium has been discounted to a greater or lesser extent by the occurrence of premelting discussed in the previous section. This conclusion is consistent with the much more pronounced increase in $t_{1/2}$ at the phase transition for PcOC12 than for PcOC6 since, as discussed in the previous section and as can be seen in Figure 12, the premelting phenomenon is more pronounced for the latter compound.

Distance and Temperature Dependence in the Mesophase. In Figure 11 the values of $t_{1/2}$ are plotted semilogarithmically against the edge-to-edge intercolumnar distance in the mesophase, R_D, for a temperature 10° above the phase transition and at 200 °C. If the data points for PcOC18 are discounted, for the reasons discussed above, reasonably good linear dependences are found, with β_R values of 0.63 and 0.65 Å^{-1}, respectively. These values are not subject to an uncertainty in the electron transfer pathway, as was the case in the solid, since the molecules are horizontally stacked and the preferred and shortest pathways for electron transfer coincide. The values are, however, subject to uncertainty as a result of the disperse decay kinetics. When values of the $1/e$ decay time Γ are plotted against R_D instead of the half-lives, the exponential distance parameter β_R decreases by approximately 20% from 0.64 to 0.52 Å^{-1}.

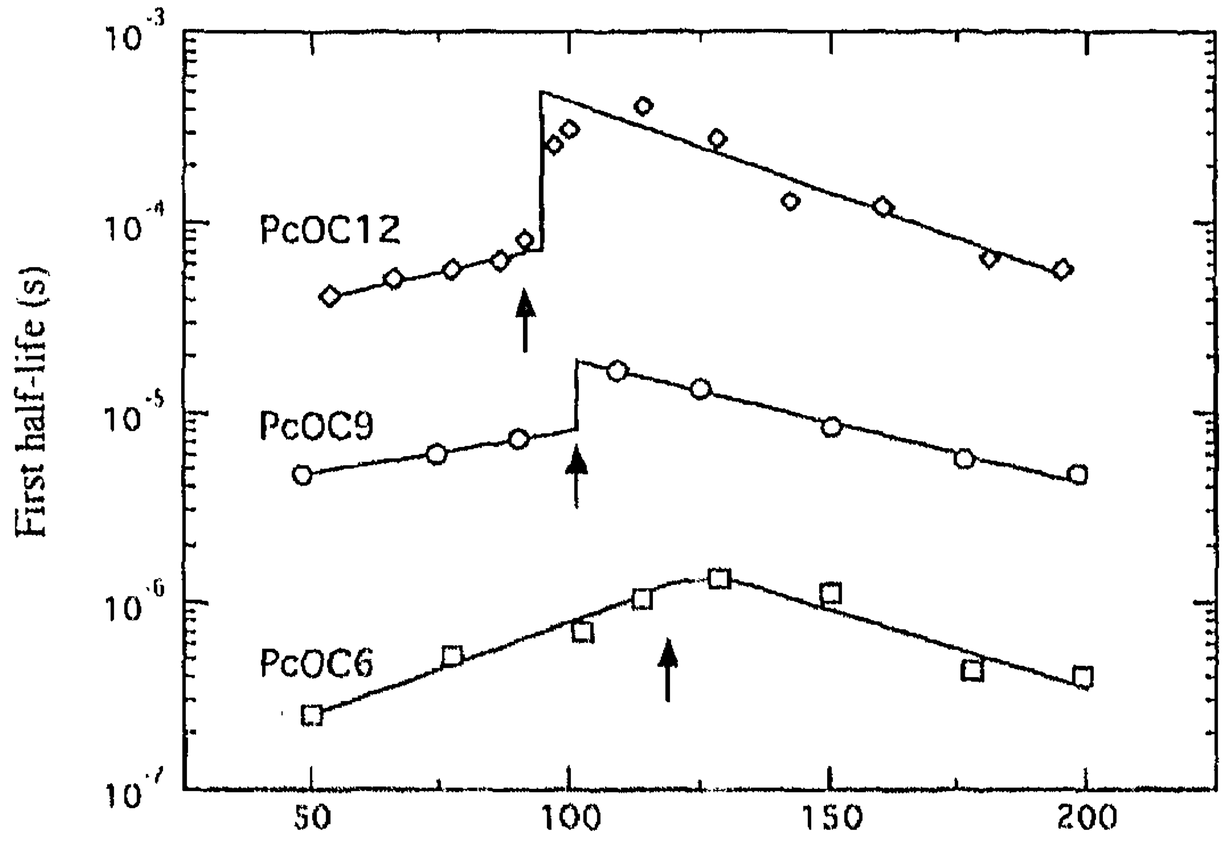

Figure 14. Temperature dependence of the first half-life of the conductivity decays for the PcOC6, -9, and -12 compounds in the region of the transition from the solid to the liquid crystalline phase at which the hydrocarbon chains melt (indicated by the vertical arrows).

While β_R is temperature independent in the mesophase, the preexponential factor τ_R in eq 19 decreases with increasing temperature, from 4.0×10^{-10} to 1.0×10^{-10} s over the *ca.* 100° temperature range studied. This corresponds to a positive activation energy of approximately 0.2 eV for the rate of charge recombination. There would appear, therefore, to be an energy barrier toward coupling to the hydrocarbon barrier in its liquid form. The eventual attenuation of the coupling within the liquid medium would however appear to be less than that for the crystalline solid on the basis of the β_R values found.

Summary

Charge recombination in pulse-irradiated columnar stacks of peripherally octa-*n*-alkoxy-substituted phthalocyanines (PcOC*n*, with *n* the alkyl chain length) is controlled by stack-to-stack electron tunneling through the saturated hydrocarbon mantle which separates the phthalocyanine cores for *n* from 5 up to at least 18 in the solid phase and at least 12 in the liquid crystalline phase. The first half-life obeys an exponential dependence on the edge-to-edge distance, R, between nearest neighbor cores, as measured by X-ray diffraction.

$$t_{1/2} = \tau_R \exp(\beta_R R) \qquad (19)$$

At low temperatures in the crystalline solid τ_R and β_R become independent of temperature and equal to 1.5×10^{-13} s and 1.10 Å^{-1}, respectively. The corresponding distance parameter expressed in terms of the total number of methylene groups separating the cores, i.e. $N = 2n$, is $\beta_N = 0.48$. If account is taken of the tilt of the molecules in the stacks and the preferred pathway for electron transfer is in the direction of the plane of the molecules, i.e. along the alkyl chains, rather than over the shortest distance, then β_R is reduced to 0.95 Å^{-1}.

The attenuation parameter is quite close to values which have been measured for rigid, saturated hydrocarbon bridges, e.g. 0.88 Å^{-1} by Paddon-Row et al.,[27] 0.9−1.1 Å^{-1} by Miller et al.,[29,32] and 1.25 Å^{-1} by Lewis et al.,[31] and recent values of 0.95 and

0.98 Å^{-1} measured for electron and hole tunneling through alkyl chains in organized thiol monolayers.[43] It is, however, much larger than the value of 0.4 Å^{-1} derived in the pioneering experimental work of Kuhn.[41] A possible reason for at least part of this discrepancy is given below.

At elevated temperatures in the solid phase, conformation fluctuations in the interfacial region of the hydrocarbon barrier cause the electron transfer rate to decrease with increasing temperature. This "premelting" effect is most pronounced for the shortest alkyl chains and illustrates how "artificially low" values of β_R can be measured for composite barriers containing both strong and weak coupling regions. This type of system is quite common in nature in the form of lipid bilayers and in laboratory systems, as, for example, in Langmuir–Blodgett films. It is possible that this is part of the explanation for the very low value of β_R reported by Kuhn and Möbius which was determined for LB films at room temperature. In the present work the effective value of β_R at room temperature in the solid phase, 0.79 Å^{-1}, is considerably lower than the limiting low-temperature value of 1.1 Å^{-1} because of fluctuations in the interfacial chain-end region which preferentially decrease the rate of electron transfer for the shorter chains at elevated temperatures.

At the transition from the solid to the mesophase the hydrocarbon chains melt completely and the barrier becomes liquid-like while the columnar order of the stacked phthalocyanines remains. Because of premelting in the solid, the recombination kinetics remain almost unchanged for the $n = 6$ compound at the transition. They do, however, become almost 1 order of magnitude slower for $n = 12$.

In the mesophase the molecules are horizontally stacked and the preferred and shortest pathways coincide. The value of β_R is independent of temperature and equal to 0.64 Å^{-1}, with a corresponding value of β_N of 0.41. The preexponential factor τ_R, however, decreases with increasing temperature in the mesophase according to $\tau_R = (6 \times 10^{-13}) \exp(0.21/k_BT)$, with k_BT in electronvolts. It would appear that while coupling into the rapidly fluctuating liquid medium involves an activation barrier, once "coupled-in", electron transfer can extend to longer distances in the liquid than in the solid on the basis of the β_R values of 0.64 and *ca.* 1.0 Å^{-1}, respectively. To our knowledge the present measurements are the first to provide information on electron tunneling through an insulating liquid barrier with a well-defined width.

The present results clearly demonstrate that long-distance electron transfer is sensitive to the nature of the intervening medium. The use still by some of the simple through-space tunneling equation which gives $\beta_R = 4\pi(2m_eV_{ab})^{0.5}/h$, with V_{ab} the barrier height, is therefore a gross oversimplification. For the present systems with a barrier height of *ca.* 3 eV, $\beta_R = 1.8$ Å^{-1} would be predicted, which is much larger than the values measured.

Many theoretical treatments of long-distance electron transfer across polymethylene chains via through-bond coupling have appeared, and estimates of β_R in the range 0.5-1.0 Å^{-1} have been calculated.[15,17–22,26,109,110] Comparison of the present results with such treatments of the influences of chain configurations and van der Waals contacts is considered to be premature and will require a more detailed understanding of the structure of the hydrocarbon barrier in these media. We hope that this will be achievable in the near future as a result of more detailed NMR and X-ray analysis. The premelting phenomenon observed and the "liquid" barrier data may perhaps be better discussed in terms of recent theoretical treatments of long-distance electron transfer in which the barrier is considered in more general terms.[47,48,111–117]

Acknowledgment. The authors would like to express their thanks to Dr. M. P. de Haas for many helpful discussions and for his innovative solutions to real-time data acquisition of complex kinetic transients. We are also indebted to Drs. J. W. Zwikker and J. F van der Pol for the synthesis of many of the compounds studied, and to Drs. M. G. Northoldt and S. J. Picken for the small angle X-ray diffraction data, which were essential for the quantitative analysis of the results.

References and Notes

(1) Kavarnos, G. J. *Fundamentals of Photoinduced Electron Transfer*; VCH: New York, 1993.
(2) Wasielewski, M. R. *Photoinduced Electron Transfer, Part A*; Elsevier: Amsterdam, 1988; Chapter 4, p 161.
(3) Closs, G. L.; Miller, J. R. *Science* **1988**, *240*, 440.
(4) Gust, D.; Moore, T. A. *Top. Curr. Chem.* **1991**, *159*, 103.
(5) Warman, J. M.; Smit, K. J.; Jonker, S. A.; Verhoeven, J. W.; Oevering, H.; Kroon, J.; Paddon-Row, M. N.; Oliver, A. M. *Chem. Phys.* **1993**, *170*, 359.
(6) Paddon-Row, M. N.; Jordan, K. D. In *Modern Models Of Bonding and Delocalisation*; Liebman, J. F., Greenberg, A., Eds.; VCH: New York, 1988; Chapter 3.
(7) Jortner, J. *Biochim. Biophys. Acta* **1980**, *594*, 193.
(8) Mikkelson, K. V.; Ratner, M. A. *Chem. Rev.* **1987**, *87*, 113.
(9) Fox, M. A. *Top. Curr. Chem.* **1991**, *159*, 67.
(10) Marcus, R. A. *Angew. Chem., Int. Ed. Engl.* **1993**, *32*, 1111.
(11) Oevering, H.; Paddon-Row, M. N.; Heppener, M.; Oliver, A. M.; Cotsaris, E.; Verhoeven, J. W.; Hush, N. S. *J. Am. Chem. Soc.* **1987**, *109*, 3258.
(12) *Chemical Kinetics: Electron Tunneling in Chemistry*; Compton, R. G., Ed.; Elsevier: Amsterdam, 1989.
(13) *Tunneling in Biological Systems*; Chance, B., Marcus, R. A., DeVault, D. C., Schreiffer, J. R., Frauenfelder, H., Sutin, N., Eds.; Academic Press: New York, 1979.
(14) *Dynamics and Mechanism of Photoinduced Electron Transfer and Related Phenomena*; Mataga, N., Okada, T., Masuhara, H., Eds.; Elsevier: Amsterdam, 1992.
(15) Hoffmann, R.; Imamura, A.; Hehre, W. J. *J. Am. Chem. Soc.* **1968**, *90*, 1499.
(16) Hoffmann, R. *Acc. Chem. Res.* **1971**, *4*, 1.
(17) Paddon-Row, M. N.; Shephard, M. J.; Jordan, K. D. *J. Phys. Chem.* **1993**, *97*, 1743.
(18) Shephard, M. J.; Paddon-Row, M. N.; Jordan, K. D. *Chem. Phys.* **1993**, *176*, 289.
(19) Shephard, M. J.; Paddon-Row, M. N.; Jordan, K. D. *J. Am. Chem. Soc.* **1994**, *116*, 5328.
(20) Liang, C.; Newton, M. D. *J. Phys. Chem.* **1992**, *96*, 2855.
(21) Liang, C.; Newton, M. D. *J. Phys. Chem.* **1993**, *97*, 3199.
(22) Curtiss, L. A.; Naleway, C. A.; Miller, J. R. *J. Phys. Chem.* **1993**, *97*, 4050.
(23) Broo, A.; Larsson, S. *Chem. Phys.* **1993**, *176*, 367.
(24) Braga, M.; Broo, A.; Larsson, S. *Chem. Phys.* **1991**, *156*, 1.
(25) Larsson, S.; Braga, M. *Chem. Phys.* **1993**, *176*, 367.
(26) Curtiss, L. A.; Naleway, C. A.; Miller, J. R. *J. Phys. Chem.* **1991**, *95*, 8434.
(27) Paddon-Row, M. N.; Oliver, A. M.; Warman, J. M.; Smit, K. J.; de Haas, M. P.; Oevering, H.; Verhoeven, J. W. *J. Phys. Chem.* **1988**, *92*, 6958.
(28) Warman, J. M.; Smit, K. J.; de Haas, M. P.; Jonker, S. A.; Paddon-Row, M. N.; Oliver, A. M.; Kroon, J.; Oevering, H.; Verhoeven, J. W. *J. Phys. Chem.* **1991**, *95*, 1979.
(29) Paulson, B.; Pramod, K.; Eaton, P.; Closs, G. L.; Miller, J. R. *J. Phys. Chem.* **1993**, *97*, 13042.
(30) Closs, G. L.; Calcaterra, L. T.; Green, N. J.; Penfield, K. W.; Miller, J. R. *J. Am. Chem. Soc.* **1986**, *90*, 3673.
(31) Stein, C. A.; Lewis, N. A.; Seitz, G. *J. Am. Chem. Soc.* **1982**, *104*, 2596.
(32) Johnson, M. D.; Miller, J. R.; Green, N. S.; Closs, G. L. *J. Phys. Chem.* **1989**, *93*, 1173.
(33) Miller, J. R.; Calcaterra, L. T.; Closs, G. L. *J. Am. Chem. Soc.* **1984**, *106*, 3047.
(34) Wasielewski, M. R.; Gaines, G. L.; O'Neil, M. P.; Svec, W. A.; Niemczyk, M. P.; Prodi, L.; Gosztola, D. In *Dynamics and Mechanism of Photoinduced Electron Transfer and Related Phenomena*; Mataga, N., Okada, T., Masuhara, H., Eds.; Elsevier: Amsterdam, 1992; p 87.
(35) Perkins, T. A.; Haiser, B. T.; Eyler, J. R.; Schanze, K. S. *J. Phys. Chem.* **1990**, *94*, 8745.

(36) Leland, B. A.; Joran, A. D.; Felker, P. M.; Hopfield, J. J.; Zewail, A. H.; Dervan, P. B. *J. Phys. Chem.* **1985**, *89*, 5571.
(37) Paddon-Row, M. N. *Acc. Chem. Res.* **1994**, *27*, 18.
(38) Heinz, R.; Rabe, J. P. *Langmuir*, in press.
(39) Möbius, D. *Ber. Bunsen-Ges. Phys. Chem.* **1978**, *82*, 848.
(40) Kuhn, H. *Pure Appl. Chem.* **1979**, *51*, 341.
(41) Kuhn, H. *J. Photochem.* **1979**, *10*, 111.
(42) Möbius, D. *Acc. Chem. Res.* **1981**, *14*, 63.
(43) Finklea, H. O.; Hanshew, D. D. *J. Am. Chem. Soc.* **1992**, *114*, 3173.
(44) Moser, C. C.; Keske, J. M.; Warncke, K.; Farid, R. S.; Dutton, P. L. *Nature* **1992**, *355*, 796.
(45) Beratan, D. N.; Onuchic, J. N.; Winkler, J. R.; Gray, H. B. *Science* **1992**, *258*, 1740.
(46) Beratan, D. N.; Betts, J. N.; Onuchic, J. N. *J. Phys. Chem.* **1992**, *96*, 2852.
(47) Evenson, J. W.; Karplus, M. *Science* **1993**, *262*, 1247.
(48) Onuchic, J. N.; Beratan, D. N.; Winkler, J. R.; Gray, H. B. *Annu. Rev. Biophys. Biomol. Struct.* **1992**, *21*, 349.
(49) Warman, J. M.; de Haas, M. P.; van der Pol, J. F.; Drenth, W. *Chem. Phys. Lett.* **1989**, *164*, 581.
(50) Schouten, P. G.; Warman, J. M.; de Haas, M. P.; Fox, M. A.; Pan, H.-L. *Nature* **1991**, *353*, 736.
(51) Schouten, P. G.; Warman, J. M.; de Haas, M. P.; van der Pol, J. F.; Zwikker, J. W. *J. Am. Chem. Soc.* **1992**, *114*, 9028.
(52) Schouten, P. G.; Warman, J. M.; de Haas, M. P.; van Nostrum, C. F.; Gelinck, G. H.; Nolte, R. J. M.; Copyn, M. J.; Zwikker, J. W.; Engel, M. K.; Hanack, M.; Chang, Y. H.; Ford, W. T. *J. Am. Chem. Soc.* **1994**, *116*, 6880.
(53) Guillon, D.; Skoulios, A.; Piechocki, C.; Simon, J.; Weber, P. *Mol. Cryst. Liq. Cryst.* **1983**, *100*, 275.
(54) van der Pol, J. F.; Zwikker, J. W.; Nolte, R. J. M.; Drenth, W. *Recl. Trav. Chim. Pays-Bas* **1988**, *107*, 615.
(55) van der Pol, J. F.; Neeleman, E.; Zwikker, J. W.; Nolte, R. J. M.; Drenth, W.; Aerts, J.; Visser, R.; Picken, S. J. *Liq. Cryst.* **1989**, *6*, 577.
(56) van der Pol, J. F. Ph.D. Thesis, University of Utrecht, 1990.
(57) Schouten, P. G. Ph.D. Thesis, Delft University of Technology, 1994.
(58) Simon, J.; Bassoul, P. In *The Phthalocyanines, Properties and Applications*; Leznoff, C. C., Lever, A. B. P., Eds.; VCH Publishers: New York, 1993; Vol. 2, p 225.
(59) Ford, W. T.; Summer, L.; Zhu, W.; Chang, Y. H.; Um, P.; Choi, H.; Heiney, P. A.; Maliszewskyj, C. *New. J. Chem.* **1994**, *18*, 495.
(60) Ohta, K.; Jacquemin, L.; Sirlin, C.; Bosio, L.; Simon, J. *New J. Chem.* **1988**, *12*, 751.
(61) *Handbook of Chemistry and Physics*; Weast, R. C., Ed.; CRC Press: Boca Raton, FL, 1988.
(62) Schouten, P. G.; van der Pol, J. F.; Zwikker, J. W.; Drenth, W.; Picken, S. J. *Mol. Cyrst. Liq. Cryst.* **1991**, *195*, 291; **1991**, *208*, 109.
(63) van Nostrum, C. F.; Bosman, A. W.; Gelinck, G. H.; Picken, S. J.; Schouten, P. G.; Warman, J. M.; Schouten, A. J.; Nolte, R. J. M. *J. Chem. Soc., Chem. Commun.* **1993**, 1120.
(64) Weber, P.; Guillon, P.; Skoulios, A. *Liq. Cryst.* **1991**, *9*, 369.
(65) Ubbelohde, A. R. *Melting and Crystal Structure*; Clarendon Press: Oxford, 1965; p 11.
(66) Linstead, R. P.; Robertson, J. M. *J. Chem. Soc.* **1936**, 1736.
(67) Rosenthal, J. *J. Chem. Educ.* **1991**, *68*, 285.
(68) Warman, J. M.; de Haas, M. P. In *Pulse Radiolysis of Irradiated Systems*; Tabata, Y., Ed.; CRC Press: Boca Raton, FL, 1991; Chapter 6.
(69) Infelta, P. P.; de Haas, M. P.; Warman, J. M. *Radiat. Phys. Chem.* **1977**, *10*, 353.
(70) Schouten, P. G.; Warman, J. M.; de Haas, M. P. *J. Phys. Chem.* **1993**, *97*, 9863.
(71) Warman, J. M. In *The Study of Fast Processes and Transient Species by Electron Pulse Radiolysis*; Baxendale, J. H., Busi, F., Eds.; Reidel: Dordrecht, 1982; p 433.
(72) Hummel, A. In *The Chemistry of Alkanes and Cycloalkanes*; Patai, S., Rappoport, Z., Eds.; John Wiley: New York, 1992; p 743.
(73) Warman, J. M.; de Haas, M. P. In *Pulse Radiolysis of Irradiated Systems*; Tabata, Y., Ed.; CRC Press: Boca Raton, FL, 1991; p 101.
(74) Warman, J. M. In *The Study of Fast Processes and Transient Species by Electron Pulse Radiolysis*; Baxendale, J. H., Busi, F., Eds.; Reidel: Dordrecht, 1982; p 129.
(75) Belarbi, Z.; Sirlin, C.; Simon, J.; André, J. J. *J. Phys. Chem.* **1989**, *93*, 8105.
(76) Adam, D.; Schumacher, P.; Simmerer, J.; Häussling, L.; Siemensmeyer, K.; Etzbach, K. H.; Ringsdorf, H.; Haarer, D. *Nature* **1994**, *371*, 141.
(77) Adam, D.; Closs, F.; Frey, T. D.; Funhoff, D.; Haarer, D.; Ringsdorf, H.; Schuhacher, P.; Siemensmeyer, K. *Phys. Rev. Lett.* **1993**, *70*, 457.
(78) Adam, D.; Haarer, D.; Closs, F.; Frey, T.; Funhoff, D.; Siemensmeyer, K.; Schuhmacher, P.; Ringsdorf, H. *Ber. Bunsen-Ges. Phys. Chem.* **1993**, *97*, 1366.
(79) Loufty, R. O.; Cheng, Y. C. *J. Chem. Phys.* **1980**, *73*, 2902.
(80) Blasse, G.; Dirksen, G. J.; Meijerink, A.; van der Pol, J. F.; Neeleman, E.; Drenth, W. *Chem. Phys. Lett.* **1989**, *154*, 420.
(81) Allen, A. O. *National Bureau of Standards Report No. NSRDS-NBS 58*, 1976.
(82) Casanovas, J.; Grob, R.; Delacroix, D.; Fuelfucei, J. P.; Blanc, D. *J. Chem. Phys.* **1981**, *75*, 4661.
(83) Casanovas, J.; Grob, R.; Sabattier, R.; Fuelfucei, J. P.; Blanc, D. *Radiat. Phys. Chem.* **1980**, *15*, 2936.
(84) Kohlrausch, F. *Pogg. Ann.* **1863**, *119*, 337.
(85) Plonka, A. *Time-Dependent Reactivity of Species in Condensed Media*; Lecture Notes in Chemistry; Springer-Verlag: Berlin, 1986.
(86) Plonka, A. *Annu. Rep. Prog. Chem.* **1988**, *85*, 47.
(87) Jortner, J. *J. Chem. Phys.* **1976**, *64*, 4860.
(88) Sarai, A. *Chem. Phys. Lett.* **1979**, *63*, 360.
(89) Hopfield, J. J. *Proc. Natl. Acad. Sci. U.S.A.* **1974**, *171*, 3640.
(90) Redi, M.; Hopfield, J. J. *J. Chem. Phys.* **1980**, *72*, 6651.
(91) Liang, N.; Miller, J. R.; Closs, G. L. *J. Am. Chem. Soc.* **1990**, *112*, 5353.
(92) Smit, K. J.; Warman, J. M.; de Haas, M. P.; Paddon-Row, M. N.; Oliver, A. M. *Chem. Phys. Lett.* **1988**, *152*, 177.
(93) Lauterwasser, C.; Finkele, U.; Scheer, H.; Zinth, W. *Chem. Phys. Lett.* **1991**, *183*, 471.
(94) Gunner, M. R.; Robertson, D. E.; Dutton, P. L. *J. Phys. Chem.* **1986**, *90*, 3783.
(95) Fleming, G. R.; Martin, J.-L.; Breton, J. *Nature* **1988**, *333*, 190.
(96) Parson, W. W. *Biochim. Biophys. Acta* **1967**, *131*, 154.
(97) Floyd, B. A.; Chance, B.; De Vault, D. *Biochim. Biophys. Acta* **1971**, *226*, 103.
(98) Hsi, E. S. P.; Bolton, J. R. *Biochim. Biophys. Acta* **1974**, *347*, 126.
(99) Hoff, A. J. *Phys. Rep.* **1979**, *54*, 75.
(100) Kentgens, A. P. M.; Markies, B. A.; van der Pol, J. F.; Nolte, R. J. M. *J. Am. Chem. Soc.* **1990**, *112*, 8800.
(101) Yang, X.; Kardan, M.; Hsu, S. L.; Collard, D.; Heath, R. B.; Lillya, C. P. *J. Phys. Chem.* **1988**, *92*, 196.
(102) Guillaume, F.; Baghdadi, A. E.; Dianoux, A. J. *Phys. Scr.* **1993**, *T49*, 691.
(103) Zerbi, G.; Magni, R.; Gussoni, M.; Moritz, K. H.; Bigotto, A.; Dirlikov, S. *J. Chem. Phys.* **1981**, *75*, 3175.
(104) Schouten, P. G.; Chen, W.; Warman, J. M.; de Haas, M. P.; van der Pol, J. F.; Zwikker, J. W. *Synth. Met.* **1991**, *42*, 2665.
(105) Schouten, P. G.; Warman, J. M.; de Haas, M. P.; Pan, H. L.; Fox, M. A. *Mol. Cryst. Liq. Cryst.* **1993**, *235*, 115.
(106) Groothues, H.; Kremer, F.; Schouten, P. G.; Warman, J. M. *Adv. Mater.* **1995**, *7*, 283.
(107) Schwiegk, S.; Werth, M.; Leisen, J.; Wegner, G.; Spiess, H. W. *Acta Polym.* **1993**, *44*, 31.
(108) Dong, R. Y.; Goldfarb, D.; Mosely, M. E.; Luz, Z.; Zimmermann, H. *J. Phys. Chem.* **1984**, *88*, 3148.
(109) McConnell, H. M. *J. Chem. Phys.* **1961**, *35*, 508.
(110) Broo, A.; Larsson, S. *Chem. Phys.* **1990**, *148*, 103.
(111) Franzen, S.; Goldstein, R. F.; Boxer, S. G. *J. Phys. Chem.* **1993**, *97*, 3040.
(112) Gudowska-Novak, E. *J. Phys. Chem.* **1994**, *98*, 5257.
(113) Mujica, V.; Kemp, M.; Ratner, M. A. *J. Chem. Phys.* **1994**, *101*, 6856.
(114) Singh, S.; Robinson, G. W. *J. Phys. Chem.* **1995**, *99*, 2764.
(115) Spears, K. G. *J. Phys. Chem.* **1995**, *99*, 2469.
(116) Reichman, D. R.; Silbey, R. J. *J. Phys. Chem.* **1995**, *99*, 2777.
(117) Felts, A. K.; Pollard, W. T.; Friesner, R. A. *J. Phys. Chem.* **1995**, *99*, 2969.

JP950995L